International Journal of Solids and Structures 000 (2016) 1–13

Contents lists available at ScienceDirect

International Journal of Solids and Structures

journal homepage: www.elsevier.com/locate/ijsolstr

Influence of a mobile incoherent interface on the strain-gradient plasticity of a thin slab

Anup Basak[a], Anurag Gupta[b,*]

[a] Department of Aerospace Engineering, Iowa State University, Ames, IA 50011, USA
[b] Department of Mechanical Engineering, Indian Institute of Technology Kanpur, U.P. 208016, India

ARTICLE INFO

Article history:
Received 8 May 2016
Revised 7 October 2016
Available online xxx

Keywords:
Strain-gradient plasticity
Incoherent interface
Interface kinetics
Material inhomogeneity
Size effects

ABSTRACT

A thermodynamically consistent theory of strain-gradient plasticity in isotropic solids with mobile incoherent interfaces is developed. The gradients of plastic strain are introduced in the yield functions, both of the bulk and the interface, through suitable measures of material inhomogeneity; consequently, two internal length scales appear in the formalism. The rate-independent associative plastic flow rules, as proposed in the framework, are coupled with the kinetic law for interface motion. The theory is used to study plastic evolution in a three-dimensional, semi-infinite, thin slab of isotropic solid with a planar incoherent interface. The average stress-strain curves are plotted for varying length scales, mobilities, and average strain-rates. The effect of slab thickness and the two internal length scales on the hardening behavior of the slab is investigated. For all the considered cases, the stress-strain curves have two distinct kinks, indicating yielding of the bulk and at the interface. Moreover, once the interface yields, and is driven to move, the curves demonstrate both softening and rate-dependent response. The softening behavior is found to be sensitive to interface mobility and average strain-rates. These observations are consistent with several experimental results in the literature.

1. Introduction

Resistance to plastic flow in the presence of interfaces and external boundaries leads to inhomogeneous strain distribution, such as that accommodated by the geometrically necessary dislocations (Nye, 1953; Ashby, 1970). The large gradients in plastic strain near the interfaces and boundaries strongly influence the effective hardening of the solid (Aifantis et al., 2006; Fleck and Willis, 2009). The role of surfaces is in particular significant in solids with micron and sub-micron characteristic length scales (Sutton and Balluffi, 2003). Strain-gradient plasticity theories (Fleck and Willis, 2009; Fleck and Hutchinson, 1997; Gao et al., 1999; Huang et al., 2000; Gurtin and Anand, 2005) have been successfully used to study plastic deformation in solids with interfaces such as those containing an elastic-plastic boundary (Gudmundson, 2004; Fredriksson and Gudmundson, 2007; 2005; Polizzotto, 2009), grain boundaries (Voyiadjis et al., 2014; Al-Rub, 2008; Aifantis et al., 2006; Aifantis and Willis, 2005; Wulfinghoff et al., 2013; Kochmann and Le, 2008; Zhang et al., 2014b), internal surfaces in composites (Fredriksson et al., 2009), phase boundaries (Mazzoni-Leduc et al., 2008; Pardoen and Massart, 2012), and interfaces between laminates (Wulfinghoff et al., 2015). Dislocation dynamics based theories have also been used to study the effects of interfaces on plastic flow (Shu and Fleck, 1999; Puri et al., 2011; Balint et al., 2008; Zhang et al., 2014b). All these investigations are however restricted to stationary interfaces. On the other hand, various experiments (Gorkaya et al., 2011; Morris et al., 2007; Chen and Gottstein, 1988; Gourdet and Montheillet, 2002; Rupert et al., 2009; Winning et al., 2001) in polycrystalline materials have suggested that interfaces remain mobile during plastic deformation, accommodating a part of the accumulated strain near the boundaries and thereby relaxing the stresses in the body. Moreover, grain boundary propagation results in grain coarsening (increase in average grain size) in polycrystalline materials, and in this process the solids have been observed to undergo strain softening (Morris et al., 2007; Chen and Gottstein, 1988; Gourdet and Montheillet, 2002). It is therefore important to formulate a plasticity model where plastic evolution, both in the bulk and at the interfaces, is coupled with interfacial kinetics. This is precisely the purpose of the present paper. In particular, we elaborate the nature of our theory through a detailed example of a plastically deforming thin slab containing a mobile interface.

The starting point of our work is a thermodynamical framework, recently proposed by the authors (Basak and Gupta, 2015a; 2015b; 2016), using which we derive a physically motivated three-

* Corresponding author.
E-mail address: ag@iitk.ac.in (A. Gupta).

http://dx.doi.org/10.1016/j.ijsolstr.2016.12.004
0020-7683/

dimensional (3D) small deformation strain-gradient plasticity theory for isotropic solids. We allow for an energetic incoherent planar interface, whose incoherency is related to the presence of defects/inhomogeneities, to propagate within the quasi-statically deforming solid. There are two novel features of our plasticity theory. First, we assume the yield function in the bulk to depend on the incompatibility tensor (Krishnan and Steigmann, 2014; Basak and Gupta, 2016), given in terms of second order gradient of plastic strain, and the yield function on the interface to depend on an analogous incompatibility measure. Such dependence, with which we introduce two internal length scales, and which is the simplest that one could use to characterize inhomogeneity in isotropic solids (Noll, 1967), is the only source of non-locality, and hence size dependence, in our formalism. Second, we propose plasticity flow rules which are coupled with interfacial kinetic laws, so that we can model the effects of interface propagation on the overall plastic behavior of the solid. The rate-independent plasticity flow rules are assumed to be associative. The rate-dependency in the model is introduced through a linear kinetic law of interface motion. We should remark here that our strain-gradient plasticity framework, even without considering interfacial effects, is distinct from those which necessarily incorporate higher order stresses (Fleck and Willis, 2009; Gao et al., 1999; Huang et al., 2000; Gurtin and Anand, 2005; Gudmundson, 2004) or those which have a first order strain-gradient dependency in the yield function (Acharya and Bassani, 1996; Bassani, 2001). Moreover, introduction of strain gradients in our theory is through the incompatibility tensor, which is a natural measure of material inhomogeneity distribution in isotropic solids (Noll, 1967). This renders our model physically motivated from the viewpoint of inhomogeneous plastic deformations at small scales.

We apply our theory to study the plastic behavior of a semi-infinite thin slab, under tensile loading, having a planar incoherent interface (see Fig. 2). The incoherency of the interface is essentially characterized by a non-trivial jump in plastic strain across the interface. In fact, for the thin slab problem, the driving force for interface propagation comes out to be proportional to this jump. As a result, interface is driven to motion within the slab only if it is incoherent. We consider two cases to illustrate our theory. First, we assume the interface to be located in the middle of the slab. The symmetry of the problem prevents incoherency and consequently any motion of the interface. The achieved simplicity however allows us to obtain an analytical solution, which is used to understand the nature of the two internal length scales as well as investigate the size effects on the overall plasticity of the slab. In the second case, we assume the interface to be located asymmetrically in the slab such that the amplitude of plastic strain in the thinner side is almost an order smaller than the other side. The interface becomes incoherent immediately after yielding and subsequently propagates into the thinner region. In both the cases, yielding in the bulk precedes that at the interface. This is reasonable since inhomogeneities (such as dislocations) pile up near the interface during bulk plastic flow, and start to rearrange abruptly at certain critical stress, leading to strain burst and eventual yielding at the interface (Morris et al., 2007; Chen and Gottstein, 1988). Once yielded, the interface encourages stress relaxation in the slab by allowing defects to transmit from one bulk region into the other. For instance, the dislocations, which get dissociated from the interface, get impinged into the adjacent bulk, and a fraction of the bulk dislocations get accumulated at the boundaries to modify their structural and mechanical behavior (cf. Chapter 12 of Sutton and Balluffi (2003)). Furthermore, if driven to move, the interface helps in further relaxation of stress by accommodating the cumulative strain in its neighborhood. Interestingly, when the interface propagates with a finite speed, the effective plastic behavior of the slab exhibits both strain softening and strain-rate dependency. The softening is more prominent for highly mobile interfaces. On the other hand, increase in the average strain-rate raises the maximum stress attained by the slab, thereby delaying the softening response. These findings are in confirmation with the available experimental observations (Morris et al., 2007; Chen and Gottstein, 1988; Legros et al., 2008).

The earliest formulation to include strain gradients within a plasticity theory was proposed by Aifantis (1984; 1987) in an attempt to develop a microstructurally informed macroscopic theory of plastic flow. Departing from the classical theories, he modified the flow stress to include a linear dependence on Laplacian of the effective plastic strain. This led to introduction of an internal length scale in the theory and eventually to an effective prediction of size dependent material response. The strain-gradient effect was alternatively introduced by Fleck et al. (1994) and Fleck and Hutchinson (1997) using the framework of couple stress theory. In a significant development, Fleck and Hutchinson (2001) used principle of virtual power to derive a broad class of strain-gradient plasticity models, where the notion of effective plastic strain was also generalized so as to introduce multiple internal length scales within the same framework. The theory was however found to be inconsistent with the laws of thermodynamics (Gurtin and Anand, 2009; Gudmundson, 2004). A thermodynamically consistent strain-gradient theory was developed, again using the principle of virtual power but incorporating a strain-gradient dependent defect energy, by Gurtin and Anand (2009). Our strain-gradient plasticity model is fundamentally different to these in that we include a dependence on second gradient of strain (through the incompatibility tensor) constitutively in the yield criteria. We do not consider contributions from defect energy, neither do we use the principle of virtual power.

The strain-gradient plasticity models for bulk deformation were extended to include interface energy in the works of Aifantis and Willis (2004; 2005; 2006). It is in these works that we find the first discussions of interfacial versus bulk yielding (Aifantis and Willis, 2005), 'knee' like feature in stress-strain relations (Aifantis and Willis, 2004), and the associated phenomena of strain burst captured through nanoindentation experiments (Aifantis et al., 2006; Aifantis and Willis, 2005). A detailed comparison between gradient plasticity models with experimental data illustrating a 'knee' is also available in their more recent works (Zhang et al., 2014a; Zhang and Aifantis, 2015). There have been several other proposals and applications of strain-gradient plasticity theories which include interfacial effects (Basak and Gupta, 2016; Al-Rub, 2008; Fleck and Willis, 2009; Fredriksson and Gudmundson, 2007; 2005; Polizzotto, 2009; Gudmundson, 2004; Gupta and Steigmann, 2012; Pardoen and Massart, 2012; Voyiadjis et al., 2014; Wulfinghoff et al., 2015; 2013). Our interfacial plasticity model is distinct from these in the way strain gradients have been incorporated in the interface yield criteria. Our dependence is motivated from the incompatibility of plastic strain at the interface. Furthermore, ours is the first strain-gradient plastic model, to the best of our knowledge, which includes mobile interfaces such as those present during phase/grain boundary propagation. In this way, we are able to study the effect of dynamic interfaces on the overall strain-gradient plasticity of the solid.

We have organized the paper as follows. A general theory of small deformation plastic flow in isotropic solids with a propagating planar incoherent interface has been developed in Section 2. It includes formulating the necessary kinematics, deriving local dissipation inequalities, and consequently proposing plastic flow rules and interfacial kinetics. In Section 3, the general theory is simplified towards posing an initial-boundary value problem for investigating the plastic deformation of a semi-infinite thin slab, as shown in Fig. 2. The problem is solved, and the results are discussed in detail, in Section 4 first for a stationary interface within

Please cite this article as: A. Basak, A. Gupta, Influence of a mobile incoherent interface on the strain-gradient plasticity of a thin slab, International Journal of Solids and Structures (2016), http://dx.doi.org/10.1016/j.ijsolstr.2016.12.004

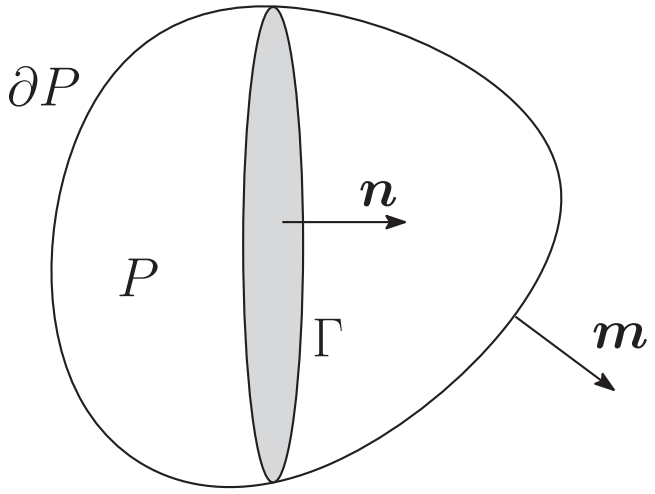

Fig. 1. A 3D region $P \subset G$ with a planar interface $\Gamma \subset C$. Here, $\boldsymbol{n}$ is the fixed unit normal to the interface and $\boldsymbol{m}$ is the outward unit normal to the boundary ∂P.

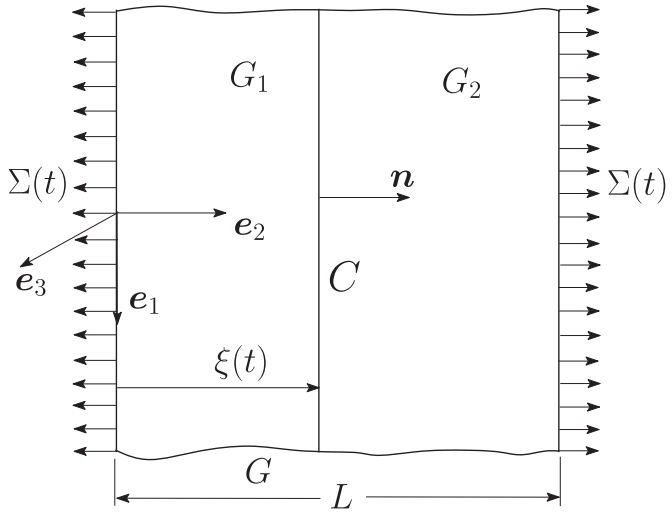

Fig. 2. A semi-infinite slab G with a planar incoherent interface C. The thickness of the slab is L, $\Sigma(t)$ is the applied stress, and $\xi(t)$ is the instantaneous position of the interface at time t.

the slab and then for a propagating interface. Finally, we conclude our work in Section 5.

2. General theory

In this section we introduce a 3D isothermal framework for developing a thermodynamically consistent small deformation elastic-plastic theory for single-phase isotropic solids with mobile incoherent interfaces. We restrict ourselves to planar interfaces with well defined normals. After introducing necessary kinematics we postulate a global dissipation inequality which, under specific constitutive assumptions on the nature of bulk and interface energy, yields local dissipation inequalities for the bulk and the interfacial region. These local relations are then used to derive both the plasticity flow rules (for bulk and interface) and the interfacial kinetic law.

The solid body under consideration occupies a subset G of the 3D Euclidean point space. It contains a singular interface C with a constant unit normal $\boldsymbol{n}$. Let $P \subset G$ be an arbitrary region in the body such that $\Gamma = P \cap C$ is nonempty (see Fig. 1). The outward unit normal to the boundary ∂P of P is denoted by $\boldsymbol{m}$. The gradient of a differentiable bulk vector field $\boldsymbol{f}$, with respect to the position in G, is a tensor field denoted as $\nabla \boldsymbol{f}$, whereas its divergence is given by $\mathrm{div}\boldsymbol{f}$. The material time derivative of $\boldsymbol{f}$ is indicated by a superposed dot. We have denoted time as t. The surface gradient and the surface divergence of a differentiable interfacial field $\boldsymbol{g}$ are denoted by $\nabla^S \boldsymbol{g}$ and $\mathrm{div}^S \boldsymbol{g}$, respectively (Cermelli and Gurtin, 1994; Gupta and Steigmann, 2012). For a piecewise continuous bulk field f, the jump and average across C are defined as $[\![f]\!] = f_+ - f_-$ and $\langle f \rangle = (f_+ + f_-)/2$, respectively, where f_+ is the limiting value of f at the interface as we approach the interface from the bulk region into which the normal $\boldsymbol{n}$ points (f_- is defined likewise). It can be easily verified that

$$[\![f_1 f_2]\!] = [\![f_1]\!]\langle f_2 \rangle + \langle f_1 \rangle [\![f_2]\!], \tag{1}$$

where f_1 and f_2 are two piecewise continuous bulk fields.

Additional notation is fixed as follows. The Euclidean inner product of two second order tensors $\boldsymbol{A}$ and $\boldsymbol{B}$ is written as $\boldsymbol{A} \cdot \boldsymbol{B}$; the related norm is denoted as $|\boldsymbol{A}|$. The trace, transpose, and inverse of $\boldsymbol{A}$ are denoted by $\mathrm{tr}\boldsymbol{A}$, $\boldsymbol{A}^T$, and $\boldsymbol{A}^{-1}$, respectively. The symmetric and skew parts of $\boldsymbol{A}$ are represented by $\mathrm{sym}(\boldsymbol{A})$ and $\mathrm{skw}(\boldsymbol{A})$, respectively. The derivative of a scalar-valued differentiable function of $\boldsymbol{A}$, say $f(\boldsymbol{A})$, denoted by $\partial_{\boldsymbol{A}} f$, is defined by $f(\boldsymbol{A}+\boldsymbol{B}) = f(\boldsymbol{A}) + \partial_{\boldsymbol{A}} f \cdot \boldsymbol{B} + o(|\boldsymbol{B}|)$, where $o(|\boldsymbol{B}|)/|\boldsymbol{B}| \to 0$ as $|\boldsymbol{B}| \to 0$. The derivatives of vector and tensor-valued differentiable functions are defined similarly. The second order identity tensor is given by $\boldsymbol{I}$.

2.1. Kinematics

Let $\boldsymbol{u}$ be a continuous displacement field defined over G. The displacement gradient tensor, $\boldsymbol{\beta} = \nabla \boldsymbol{u}$, is however allowed to be discontinuous across C. The infinitesimal strain tensor field and the spin tensor field, well defined away from C, are $\boldsymbol{\epsilon} = \mathrm{sym}(\boldsymbol{\beta})$ and $\boldsymbol{\omega} = \mathrm{skw}(\boldsymbol{\beta})$, respectively. The following decomposition of $\boldsymbol{\beta}$ into an elastic part $\boldsymbol{\beta}^e$ and a plastic part $\boldsymbol{\beta}^p$ is assumed (Kröner, 1981):

$$\boldsymbol{\beta} = \boldsymbol{\beta}^e + \boldsymbol{\beta}^p. \tag{2}$$

The above considerations are justified if we assume $\boldsymbol{\beta}$, $\boldsymbol{\beta}^e$, and $\boldsymbol{\beta}^p$ to be small (of the same order). Consequently, the total strain and total spin are also decomposed into elastic and plastic parts as

$$\boldsymbol{\epsilon} = \boldsymbol{\epsilon}^e + \boldsymbol{\epsilon}^p \quad \text{and} \quad \boldsymbol{\omega} = \boldsymbol{\omega}^e + \boldsymbol{\omega}^p, \tag{3}$$

where the notation is self explanatory. It is immediate that $\boldsymbol{\epsilon}^e = \mathrm{sym}(\boldsymbol{\beta}^e)$, $\boldsymbol{\epsilon}^p = \mathrm{sym}(\boldsymbol{\beta}^p)$, $\boldsymbol{\omega}^e = \mathrm{skw}(\boldsymbol{\beta}^e)$, and $\boldsymbol{\omega}^p = \mathrm{skw}(\boldsymbol{\beta}^p)$.

The continuity of $\boldsymbol{u}$ requires $[\![\boldsymbol{u}]\!] = \boldsymbol{0}$, which implies $[\![\boldsymbol{\beta}]\!]\boldsymbol{P} = \boldsymbol{0}$, where $\boldsymbol{P} = \boldsymbol{I} - \boldsymbol{n} \otimes \boldsymbol{n}$ is the projection tensor ($\otimes$ denotes the dyadic product). The interfacial distortion tensor field can then be unambiguously defined as $\boldsymbol{G} = \boldsymbol{\beta}_+ \boldsymbol{P} = \boldsymbol{\beta}_- \boldsymbol{P} = \langle \boldsymbol{\beta} \rangle \boldsymbol{P}$ (Gupta and Steigmann, 2012). The interfacial strain field, defined as $\boldsymbol{E} = \mathrm{sym}(\boldsymbol{G})$, is related to the bulk strain field as $\boldsymbol{E} = \boldsymbol{P}\langle \boldsymbol{\epsilon} \rangle \boldsymbol{P}$. Analogous to the decomposition (2) in the bulk, the interfacial distortion is additively decomposed into elastic and plastic parts as

$$\boldsymbol{G} = \boldsymbol{G}^e_\gamma + \boldsymbol{G}^p_\gamma = \boldsymbol{G}^e_\delta + \boldsymbol{G}^p_\delta, \tag{4}$$

where $\boldsymbol{G}^e_\gamma = \boldsymbol{\beta}^e_+ \boldsymbol{P}$, $\boldsymbol{G}^e_\delta = \boldsymbol{\beta}^e_- \boldsymbol{P}$, $\boldsymbol{G}^p_\gamma = \boldsymbol{\beta}^p_+ \boldsymbol{P}$, and $\boldsymbol{G}^p_\delta = \boldsymbol{\beta}^p_- \boldsymbol{P}$; see Gupta and Steigmann (2012) and Basak and Gupta (2016) for the corresponding multiplicative decomposition when the deformations are finite. Here, the subscripts δ and γ have been used to differentiate the two disjoint surfaces obtained from the incoherent interface in the intermediate configuration (Gupta and Steigmann, 2012; Basak and Gupta, 2016). The decomposition of the interfacial strain tensor follows subsequently as

$$\boldsymbol{E} = \boldsymbol{E}^e_\gamma + \boldsymbol{E}^p_\gamma = \boldsymbol{E}^e_\delta + \boldsymbol{E}^p_\delta, \tag{5}$$

where $\boldsymbol{E}^e_\gamma = \boldsymbol{P}\boldsymbol{\epsilon}^e_+ \boldsymbol{P}$, $\boldsymbol{E}^e_\delta = \boldsymbol{P}\boldsymbol{\epsilon}^e_- \boldsymbol{P}$, $\boldsymbol{E}^p_\gamma = \boldsymbol{P}\boldsymbol{\epsilon}^p_+ \boldsymbol{P}$, and $\boldsymbol{E}^p_\delta = \boldsymbol{P}\boldsymbol{\epsilon}^p_- \boldsymbol{P}$ are respective interfacial elastic and plastic strain fields. The incoherency

Please cite this article as: A. Basak, A. Gupta, Influence of a mobile incoherent interface on the strain-gradient plasticity of a thin slab, International Journal of Solids and Structures (2016), http://dx.doi.org/10.1016/j.ijsolstr.2016.12.004

tensor, which measures the relative elastic (or plastic) distortion between γ and δ sides of the interface, is given by

$$\boldsymbol{M} = \boldsymbol{G}^e_\delta - \boldsymbol{G}^e_\gamma = \boldsymbol{G}^p_\gamma - \boldsymbol{G}^p_\delta, \tag{6}$$

cf. Gupta and Steigmann (2012) and Cermelli and Gurtin (1994) for definition of the incoherency tensor in the finite deformation framework. For a coherent interface, $\boldsymbol{G}^e_\delta = \boldsymbol{G}^e_\gamma$ and $\boldsymbol{G}^p_\gamma = \boldsymbol{G}^p_\delta$, the incoherency tensor vanishes identically.

Let g be a smooth field defined over the interface C. The normal time derivative of g following C is given by Gurtin and Jabbour (2002)

$$\mathring{g} = \dot{g} + V\nabla g \cdot \boldsymbol{n}, \tag{7}$$

where V is the normal velocity field of the interface. It quantifies the rate of change of g as observed by an observer sitting on the moving interface. The parametrization independent intrinsic velocity of the edge $\partial\Gamma$ of Γ is given by Gurtin and Jabbour (2002)

$$\boldsymbol{q} = V\boldsymbol{n} + W\boldsymbol{t}, \tag{8}$$

where W is the component of the edge velocity along a direction (quantified with unit vector $\boldsymbol{t}$) which is both tangential to the interface and normal to the curve $\partial\Gamma$.

2.2. Dissipation inequality

Recall region P as introduced in the beginning of Section 2 and shown in Fig. 1. Assuming that P does not exchange mass with its surrounding, and neglecting excess mass density at the interface, we have the following local mass balance laws: $\dot{\rho} = 0$ in $G\backslash C$ and $V[\![\rho]\!] = 0$ over C, where ρ is the mass density of the bulk (Gupta and Steigmann, 2012). These imply that density is time independent and continuous across the singular interface, allowing the interface to be mobile. The linear momentum balance for the region P, while neglecting interfacial stresses, body forces, and inertia, yields (Gupta and Steigmann, 2012)

$$\operatorname{div}\boldsymbol{\sigma} = \boldsymbol{0} \text{ in } G\backslash C \quad \text{and} \quad [\![\boldsymbol{\sigma}]\!]\boldsymbol{n} = \boldsymbol{0} \text{ over } C, \tag{9}$$

where $\boldsymbol{\sigma}$ is the symmetric bulk Cauchy stress tensor.

According to a mechanical version of the second law of thermodynamics, the rate of change of the total free energy of P is always less than or equal to the net power input into P. Neglecting kinetic energies of the bulk and interface, we postulate the dissipation inequality as (Basak and Gupta, 2015a; 2015b; 2016)

$$\frac{d}{dt}\left(\int_P \Psi\, dv + \int_\Gamma \Phi\, da\right) \le \int_{\partial P} \boldsymbol{\sigma}\boldsymbol{m}\cdot\boldsymbol{v}\, da + \int_{\partial\Gamma} \boldsymbol{c}\cdot\boldsymbol{q}\, dl. \tag{10}$$

Here Ψ is the free energy in the bulk per unit volume, Φ is the free energy of the interface per unit area, $\boldsymbol{v}$ is the material velocity field, dv is an infinitesimal volume element, da is an infinitesimal area element, and dl is an infinitesimal length element. The first term on the right hand side of the inequality denotes the mechanical power input to P through the working of traction on the outer surface ∂P. The second term is a non-standard power input to P considered to ensure that the entropy production is restricted only to within the bulk and interface, i.e., there is no entropy generation at the arbitrary edge of the interface $\partial\Gamma$ (Basak and Gupta, 2015a; 2015b; 2016). The exact form of $\boldsymbol{c}$ will depend on the constitutive form of the energies. Using the standard transport relations and divergence theorems, inequality (10) can be rewritten as

$$\int_P \left(\operatorname{div}(\boldsymbol{\sigma}\boldsymbol{v}) - \dot{\Psi}\right) dv + \int_\Gamma \left(V[\![\Psi]\!] + [\![\boldsymbol{\sigma}\boldsymbol{v}]\!]\cdot\boldsymbol{n} - \mathring{\Phi}\right) da + \int_{\partial\Gamma} (\boldsymbol{c}\cdot\boldsymbol{q} - \Phi W)\, dl \ge 0. \tag{11}$$

The last term on the left hand side of the inequality should vanish identically, since otherwise it will represent an unphysical contribution to the entropy. Considering energies of the form $\Psi = \hat{\Psi}(\boldsymbol{\epsilon}^e)$ and $\Phi = \hat{\Phi}(\boldsymbol{M})$, we thereby require $\boldsymbol{c}\cdot\boldsymbol{n} = 0$ and $\boldsymbol{c}\cdot\boldsymbol{t} = \Phi$. Additionally, we assume plastic incompressiblity (i.e., $\operatorname{tr}\boldsymbol{\epsilon}^p = 0$). The global dissipation inequality (11) can then be shown to be equivalent to the constitutive relation $\boldsymbol{\sigma} = \partial_{\boldsymbol{\epsilon}^e}\hat{\Psi}$ and the local dissipation inequalities

$$\boldsymbol{\sigma}^d \cdot \dot{\boldsymbol{\epsilon}}^p \ge 0 \text{ in } G\backslash C \quad \text{and} \tag{12}$$

$$V f_n - \boldsymbol{B}\cdot\mathring{\boldsymbol{M}} \ge 0 \text{ over } C, \tag{13}$$

where $\boldsymbol{\sigma}^d = \boldsymbol{\sigma} - (\operatorname{tr}\boldsymbol{\sigma})\boldsymbol{I}/3$ is the deviatoric part of $\boldsymbol{\sigma}$, $\boldsymbol{B} = \partial_{\boldsymbol{M}}\hat{\Phi}$, and

$$f_n = [\![\hat{\Psi}\boldsymbol{I} - \boldsymbol{\beta}^T\boldsymbol{\sigma}]\!]\boldsymbol{n}\cdot\boldsymbol{n} \tag{14}$$

is the driving force for interface propagation (Basak and Gupta, 2016; Gupta and Steigmann, 2012). According to (12), dissipation in the bulk is only due to plastic evolution, whereas dissipation at the interface is an outcome of both the kinetics of interfacial motion as well as the evolution of the incoherency tensor.

To be more specific, we use quadratic energy densities which, after considerations of isotropic material symmetry, have a general form

$$\hat{\Psi}(\boldsymbol{\epsilon}^e) = \frac{\lambda}{2}(\operatorname{tr}\boldsymbol{\epsilon}^e)^2 + \mu\,\boldsymbol{\epsilon}^e\cdot\boldsymbol{\epsilon}^e \quad \text{and} \tag{15}$$

$$\hat{\Phi}(\boldsymbol{M}) = \Phi_0 + \frac{b_0}{2}(\operatorname{tr}\boldsymbol{M}_s)^2 + b_1(|\boldsymbol{M}_s|^2 + |\boldsymbol{M}_a|^2), \tag{16}$$

where λ and μ are the Lamé constants in the bulk, b_0 and b_1 are the moduli of incoherency for the interface, $\boldsymbol{M}_s = \operatorname{sym}(\boldsymbol{M})$, $\boldsymbol{M}_a = \operatorname{skw}(\boldsymbol{M})$, and Φ_0 is the constant interfacial tension. From these expressions we can obtain

$$\boldsymbol{\sigma} = \lambda(\operatorname{tr}\boldsymbol{\epsilon}^e)\boldsymbol{I} + 2\mu\boldsymbol{\epsilon}^e \quad \text{and} \tag{17}$$

$$\boldsymbol{B} = b_0(\operatorname{tr}\boldsymbol{M}_s)\boldsymbol{P} + 2b_1(\boldsymbol{M}_s + \boldsymbol{M}_a). \tag{18}$$

Finally, if $\boldsymbol{M}_a = \boldsymbol{0}$ then, noting that $\boldsymbol{M}_s = \boldsymbol{E}^p_\gamma - \boldsymbol{E}^p_\delta$, we can rewrite (13) as

$$V f_n - \boldsymbol{B}\cdot\mathring{\boldsymbol{E}}^p_\gamma + \boldsymbol{B}\cdot\mathring{\boldsymbol{E}}^p_\delta \ge 0 \text{ over } C. \tag{19}$$

2.3. Plastic flow rules and interfacial kinetics

Based on dissipation inequalities (12) and (19) we now derive the plastic flow rules, both in the bulk and at the interface, and interfacial kinetic equations. The plastic evolution will be assumed to be rate-independent and associative. We will depart from classical plasticity by assuming the yield functions to depend on measures of material inhomogeneity, represented in terms of suitable gradients of plastic strain. Such dependence is the only source of strain-gradient effects in our theory.

2.3.1. Bulk plasticity

In order to incorporate non-locality in our plasticity model, we assume the yield function to depend on a suitable measure of material inhomogeneity, besides its usual dependence on stress and effective plastic strain. It is well established (Noll, 1967; Basak and Gupta, 2016; Krishnan and Steigmann, 2014) that, under isotropic material symmetry, material inhomogeneity is unambiguously represented by the material curvature tensor (whose vanishing provides necessary conditions for strain compatibility). When the strains are small, as is presently the case, the material curvature reduces to Kröner's incompatibility tensor $\boldsymbol{\eta} = \operatorname{curl}\operatorname{curl}\boldsymbol{\epsilon}^p$ (Kröner, 1981). With this in mind, we consider the yield locus in the deviatoric stress space (parametrized by effective plastic strain and incompatibility tensor) to be given by $\mathcal{F} = 0$, where

$$\mathcal{F} = \tilde{\mathcal{F}}(\boldsymbol{\sigma}^d, E^p, \boldsymbol{\eta}). \tag{20}$$

Please cite this article as: A. Basak, A. Gupta, Influence of a mobile incoherent interface on the strain-gradient plasticity of a thin slab, International Journal of Solids and Structures (2016), http://dx.doi.org/10.1016/j.ijsolstr.2016.12.004

In the above equation, $E^p = \int_0^t \dot{E}^p d\tau$ is the effective plastic strain with $\dot{E}^p = \sqrt{\left(2\dot{\boldsymbol{\epsilon}}^p \cdot \dot{\boldsymbol{\epsilon}}^p\right)/3}$. Under the assumption of isotropic response, $\tilde{\mathcal{F}}$ can depend on $\boldsymbol{\sigma}^d$ and $\boldsymbol{\eta}$ only through their principal invariants. We will in fact consider yield functions which are functions of only the second invariant of $\boldsymbol{\sigma}^d$ (the first invariant of $\boldsymbol{\sigma}^d$ is trivially zero) and the first invariant of $\boldsymbol{\eta}$ (denoted by η), i.e.,

$$\mathcal{F} = \hat{\mathcal{F}}(\sigma_e, E^p, \eta), \tag{21}$$

where $\sigma_e = \sqrt{\left(3\boldsymbol{\sigma}^d \cdot \boldsymbol{\sigma}^d\right)/2}$. The principle of maximum dissipation, in conjunction with (12), yields the associative flow rule

$$\dot{\boldsymbol{\epsilon}}^p = \dot{\beta}\, \partial_{\boldsymbol{\sigma}^d} \hat{\mathcal{F}}, \tag{22}$$

where $\dot{\beta} \geq 0$ is the plastic multiplier. The consistency condition $\dot{\beta}\dot{\hat{\mathcal{F}}} = 0$ will result into a second order partial differential equation (PDE) for the plastic strain-rates whenever $\dot{\beta} > 0$. The boundary conditions required for solving the PDE are provided by the flow rules at the interface and the microscopic conditions on the plastic strain-rate and/or their spatial derivative at the external boundaries of the solid, as discussed next.

2.3.2. Interfacial kinetics and interfacial flow rules

To derive the plastic flow rules and the kinetic relation we start with conditions

$$V f_n \geq 0 \quad \text{and} \quad \boldsymbol{B}_\gamma \cdot \mathring{\boldsymbol{E}}^p_\gamma + \boldsymbol{B}_\delta \cdot \mathring{\boldsymbol{E}}^p_\delta \geq 0 \quad \text{over } C, \tag{23}$$

which are sufficient for dissipation inequality (19). Here we have introduced $\boldsymbol{B}_\gamma = -\boldsymbol{B}$ and $\boldsymbol{B}_\delta = \boldsymbol{B}$. The interface C is assumed to be homophase, requiring dissipation inequality $(23)_2$ to be symmetric with respect to suffixes γ and δ. This is indeed true as can be verified using (18) in the inequality. Although we have decoupled the dissipation inequalities pertaining to interface kinetics and interface plasticity, the two phenomena remain coupled to each other due to the nature of normal time derivatives.

Motivated by dissipation inequality $(23)_1$ we postulate a linear kinetic relation of the form

$$V = M f_n, \tag{24}$$

where $M \geq 0$ is the constant interface mobility and f_n is given by (14).

Analogous to our considerations in the bulk, we assume the yield function at the interface to depend on generalized stresses $\boldsymbol{B}_\gamma$ and $\boldsymbol{B}_\delta$, parameterized by the effective interfacial plastic strain e^p, and an appropriate measure of material inhomogeneity $\boldsymbol{\kappa}$. The yield locus is given by $\mathcal{G} = 0$, where

$$\mathcal{G} = \tilde{\mathcal{G}}(\boldsymbol{B}_\gamma, \boldsymbol{B}_\delta, e^p, \boldsymbol{\kappa}). \tag{25}$$

Here $e^p = \int_0^t \mathring{e}^p d\tau$ with $\mathring{e}^p = \sqrt{|\mathring{\boldsymbol{E}}^p_\gamma|^2 + |\mathring{\boldsymbol{E}}^p_\delta|^2}$ (Basak and Gupta, 2016). For $\boldsymbol{\kappa}$, under small strain assumption, we look for a representation of the incompatibility tensor on the interface. Toward this end, we consider a closed curve C_1 in P such that it encloses an area A_1 and intersects Γ at two points. Let C_2 be the line of intersection of A_1 with Γ. The Stokes' theorem for a piecewise smooth field $\operatorname{curl} \boldsymbol{\epsilon}^p$ then yields (Gupta and Steigmann, 2012)

$$\oint_{C_1} \operatorname{curl} \boldsymbol{\epsilon}^p \, d\boldsymbol{x} = \int_{A_1} (\operatorname{curl} \operatorname{curl} \boldsymbol{\epsilon}^p)^T \boldsymbol{N} \, da - \int_{C_2} [\![\operatorname{curl} \boldsymbol{\epsilon}^p]\!] \, d\boldsymbol{x}, \tag{26}$$

where $\boldsymbol{N}$ is the unit normal to A_1. Define $\boldsymbol{\kappa}$ such that $[\![\operatorname{curl} \boldsymbol{\epsilon}^p]\!] \, d\boldsymbol{x} = -\boldsymbol{\kappa}^T \boldsymbol{t}_1 dl$, where $\boldsymbol{t}_1$ is the unit tangent along C_2. Hence

$$\boldsymbol{\kappa}^T = [\![\operatorname{curl} \boldsymbol{\epsilon}^p]\!] (\boldsymbol{t}_1 \otimes \boldsymbol{t}_2 - \boldsymbol{t}_2 \otimes \boldsymbol{t}_1), \tag{27}$$

where $\boldsymbol{t}_2$ is a unit vector on the tangential plane of the interface such that $\{\boldsymbol{t}_1, \boldsymbol{t}_2, \boldsymbol{n}\}$ form a positively oriented orthonormal basis. It is immediately clear that vanishing of incompatibility tensor, i.e., $\operatorname{curl} \operatorname{curl} \boldsymbol{\epsilon}^p = \boldsymbol{0}$, is not sufficient to ensure path independence of the closed integral in (26), which is otherwise required for imposing continuity of the displacement field (cf. pages 84–100 from Boley and Weiner, 1997). The additional condition is provided by the last integral in (26), which essentially requires vanishing of $\boldsymbol{\kappa}$ over the interface; hence $\boldsymbol{\kappa}$ can be regarded as an interfacial incompatibility measure. It can be easily checked that $\boldsymbol{\kappa}$, as defined in (27), is independent of the choice of basis vectors $\boldsymbol{t}_1$ and $\boldsymbol{t}_2$ (Gupta and Steigmann, 2012).

For our purposes in the following sections, we restrict ourselves to yield functions of the form

$$\mathcal{G} = \hat{\mathcal{G}}(\tau_e, e^p, \kappa), \tag{28}$$

where $\tau_e = \sqrt{|\boldsymbol{B}_\gamma|^2 + |\boldsymbol{B}_\delta|^2}$ is the effective stress, and κ is the first principal invariant of $\boldsymbol{\kappa}$. The postulation of maximum dissipation, in conjunction with (23), yields the associative flow rules

$$\mathring{\boldsymbol{E}}^p_\gamma = \mathring{\zeta}\, \partial_{\boldsymbol{B}_\gamma} \hat{\mathcal{G}} \quad \text{and} \quad \mathring{\boldsymbol{E}}^p_\delta = \mathring{\zeta}\, \partial_{\boldsymbol{B}_\delta} \hat{\mathcal{G}}, \tag{29}$$

where $\mathring{\zeta} \geq 0$ is the plastic multiplier for the interface. The consistency condition $\mathring{\zeta}\,\mathring{\hat{\mathcal{G}}} = 0$, combined with flow rules (29) and kinetic relation (24), can be solved to evaluate plastic strain-rates at the interface. These serve as the boundary conditions for the PDE obtained from the consistency condition in the bulk.

3. Slab with a propagating interface

The body G is now taken to be a semi-infinite thin slab with a moving planar interface C having fixed orientation $\boldsymbol{n} = \boldsymbol{e}_2$, see Fig. 2. The interface divides the slab into two parts G_1 and G_2. The components of the position vector $\boldsymbol{x}$ are denoted by x, y, and z with respect to Cartesian basis vectors $\boldsymbol{e}_1$, $\boldsymbol{e}_2$, and $\boldsymbol{e}_3$, respectively. The slab is subjected to uniform uniaxial tensile force $\Sigma(t)$ at the free boundary. The instantaneous position of the interface is denoted by $y = \xi(t)$. In the following we simplify the plasticity model, proposed in Section 2.3, under additional kinematical and constitutive assumptions and collect the governing equations for the initial-boundary value plasticity problem. The solution to the semi-infinite thin slab problem, as discussed in the following sections, can be related to several problems of practical interest, such as a bicrystal subjected to external loading (Al-Rub, 2008) or a thin film on a substrate under external loading (Fredriksson and Gudmundson, 2007; 2005).

We consider a displacement field such that only ϵ_{22} is non-trivial while all other components of the total strain remain identically zero. We assume all the fields, including strains and stresses, to be independent of coordinates x and z. We also assume the shear components of elastic and plastic strains to be zero. Additionally, elastic and plastic spin tensor fields are both assumed to vanish, yielding $\boldsymbol{M}_a = \boldsymbol{0}$. Moreover, the symmetry of the problem allows us to assume $\epsilon^e_{11} = \epsilon^e_{33}$ and $\epsilon^p_{11} = \epsilon^p_{33}$. We denote ϵ_{22} and ϵ^p_{22} as ϵ and ϵ^p, respectively. The plastic incompressibility can then be used to obtain $\epsilon^p_{11} = \epsilon^p_{33} = -\epsilon^p/2$. This result, when combined with strain decomposition $(3)_1$, yields $\epsilon^e_{11} = \epsilon^e_{33} = \epsilon^p/2$ and $\epsilon^e_{22} = \epsilon - \epsilon^p$. The non-trivial components of the bulk stress can be obtained from (17) as

$$\sigma_{11} = \sigma_{33} = \lambda\epsilon + \mu\epsilon^p \quad \text{and} \quad \sigma_{22} = (\lambda + 2\mu)\epsilon - 2\mu\epsilon^p. \tag{30}$$

On the other hand, equilibrium Eq. $(9)_1$ can be used to write $\sigma_{22} = \Sigma(t)$. The components of the deviatoric stresses can then be expressed as

$$\sigma^d_{11} = \sigma^d_{33} = -\sigma^d_{22}/2 \quad \text{and} \quad \sigma^d_{22} = \mathcal{A}\Sigma - \mathcal{B}\epsilon^p, \tag{31}$$

where

$$\mathcal{A} = \frac{4\mu}{3(\lambda + 2\mu)} \quad \text{and} \quad \mathcal{B} = \frac{2\mu(3\lambda + 2\mu)}{3(\lambda + 2\mu)}. \tag{32}$$

Please cite this article as: A. Basak, A. Gupta, Influence of a mobile incoherent interface on the strain-gradient plasticity of a thin slab, International Journal of Solids and Structures (2016), http://dx.doi.org/10.1016/j.ijsolstr.2016.12.004

To obtain equations of bulk plasticity, we begin by noting the simplified expressions for effective stress $\sigma_e = 3|\sigma^d_{22}|/2 = 3|\mathcal{A}\Sigma - \mathcal{B}\epsilon^p|/2$, equivalent plastic strain-rate $\dot{E}^p = |\dot{\epsilon}^p|$, and first invariant of incompatibility tensor $\eta = -\partial^2\epsilon^p/\partial y^2$. Moreover, we assume the yield function (21) to be a linear function of all its arguments, i.e.,

$$\mathcal{F} = \sigma_e - (K + HE^p + c\,\eta), \tag{33}$$

where K is the constant flow stress, H is the plastic modulus, and c is a phenomenological constant with a unit of force. This form reduces to a yield function in classical plasticity theory if the coefficient c, associated with the non-local term, vanishes identically. The flow rule (22) now reduces to

$$\dot{\epsilon}^p = \dot{\beta}\,\mathrm{sign}(\mathcal{A}\Sigma - \mathcal{B}\epsilon^p), \tag{34}$$

where sign(x) is equal to -1 if $x < 0$, 0 if $x = 0$, and 1 if $x > 0$. When $\dot{E}^p > 0$, the consistency condition $\dot{E}^p\dot{\mathcal{F}} = 0$ yields

$$\frac{3}{2}\,\mathrm{sign}(\mathcal{A}\,\Sigma - \mathcal{B}\,\epsilon^p)(\mathcal{A}\dot{\Sigma} - \mathcal{B}\dot{\epsilon}^p) - H|\dot{\epsilon}^p| + c\frac{\partial^2\dot{\epsilon}^p}{\partial y^2} = 0, \tag{35}$$

which is a PDE for $\dot{\epsilon}^p$. This is to be supplemented with the boundary conditions at the interface and the external boundaries $y = 0, L$, as derived in the following.

The kinetics of the interface is governed by (24) where the driving force f_n, given by (14), is now of the form

$$f_n = \frac{\mu(3\lambda + 2\mu)}{2(\lambda + 2\mu)}[\![(\epsilon^p)^2]\!] - \frac{2\mu\,\Sigma}{\lambda + 2\mu}[\![\epsilon^p]\!]. \tag{36}$$

To derive plasticity equations at the interface we begin by assuming the yield function (28) to be linear in terms of its arguments, i.e.,

$$\mathcal{G} = \tau_e - (k_0 + h_0 e^p + c_0\kappa), \tag{37}$$

where k_0 is the yield strength, h_0 is the plastic modulus, and c_0 is a material constant whose physical interpretation would be discussed later. Note that k_0 is similar to interfacial tension Φ_0 in that it resists the plastic flow near the interface (Aifantis et al., 2006). Furthermore, with $\boldsymbol{E}^e_\gamma = (\epsilon^p_+/2)\boldsymbol{P}$, $\boldsymbol{E}^e_\delta = (\epsilon^p_-/2)\boldsymbol{P}$, $\boldsymbol{E}^p_\gamma = -(\epsilon^p_+/2)\boldsymbol{P}$, $\boldsymbol{E}^p_\delta = -(\epsilon^p_-/2)\boldsymbol{P}$, and $\boldsymbol{M} = -\big((\epsilon^p_+ - \epsilon^p_-)/2\big)\boldsymbol{P}$, we can write $\boldsymbol{B} = -(b_0 + b_1)(\epsilon^p_+ - \epsilon^p_-)\boldsymbol{P}$ and consequently obtain

$$\tau_e = 2|(b_0 + b_1)(\epsilon^p_+ - \epsilon^p_-)| \tag{38}$$

and

$$\dot{e}^p = \frac{1}{\sqrt{2}}\sqrt{(\dot{\epsilon}^p_+)^2 + (\dot{\epsilon}^p_-)^2}. \tag{39}$$

Also, $\kappa = -[\![\partial\epsilon^p/\partial y]\!]$ (considering $\boldsymbol{t}_1 = \boldsymbol{e}_3$ and $\boldsymbol{t}_2 = \boldsymbol{e}_1$ in (27)). When $\boldsymbol{B}$ is non-vanishing, i.e., $\epsilon^p_+ \neq \epsilon^p_-$, flow rules (29) are reduced to

$$\mathring{\epsilon}^p_+ = \mathring{\zeta}T \quad \text{and} \quad \mathring{\epsilon}^p_- = -\mathring{\zeta}T, \tag{40}$$

where $T = -\mathrm{sign}((b_0 + b_1)(\epsilon^p_+ - \epsilon^p_-))$. On substituting these into (39) we get $\mathring{\zeta} = \mathring{e}^p$, and from consistency condition $\mathring{\zeta}\,\mathring{\mathcal{G}} = 0$ (for $\mathring{\zeta} > 0$) we obtain

$$\mathring{\zeta} = \frac{c_0}{h_{\mathrm{eff}}}\left[\!\!\left[\overline{\partial\epsilon^p/\partial y}^{\,\circ}\right]\!\!\right], \tag{41}$$

where $h_{\mathrm{eff}} = h_0 + 4(b_0 + b_1)$ is an effective measure of plastic modulus of the interface. These relations, upon using the definition of normal time derivative, can be used to solve for plastic strain-rates at the interface, which provides us with boundary conditions at the interface $y = \xi$ required for solving (35).

In the above framework nontrivial kinetic and flow relations are obtained only when the interface is incoherent, i.e., when $\epsilon^p_+ \neq \epsilon^p_-$. This can be seen by identical vanishing of both the driving force (and hence V) and strain-rates in (36) and (40). If the interface is coherent then we would still like to obtain an expression for plastic strain-rate at an otherwise stationary interface. We do so by using the consistency condition $\dot{\mathcal{G}} = 0$ (when $|\dot{\epsilon}^p_+| = |\dot{\epsilon}^p_-| > 0$) which, with the help of (37) and (39), reduces to

$$|\dot{\epsilon}^p_+| = |\dot{\epsilon}^p_-| = \frac{c_0}{h_0}[\![\partial\dot{\epsilon}^p/\partial y]\!]. \tag{42}$$

The above relations provide boundary conditions at $y = \xi$ for solving (35) when the plastic strain is continuous at the interface.

The interfacial conditions derived above should be supplemented with boundary conditions at the external surface. Following standard practice (Anand et al., 2005), we assume the external surfaces at $y = 0, L$ to be non-dissipative and properly coated so that they behave as microscopically hard boundaries, i.e.,

$$\dot{\epsilon}^p = 0 \quad \text{at } y = 0, L. \tag{43}$$

Furthermore, we assume that there is no residual plastic strain (at the initial time) in the bulk, interface, and external boundaries,

$$\epsilon^p(y, 0) = 0 \quad \text{for } 0 \le y \le L. \tag{44}$$

To summarize, the complete initial-boundary value problem for ϵ^p includes simultaneously solving (34) and (35) with the initial condition (44) and the boundary conditions (43). To these we should add conditions (40)-(41), when $\epsilon^p_+ \neq \epsilon^p_-$, or (42), when $\epsilon^p_+ = \epsilon^p_-$.

4. Results and discussion

The initial-boundary value problem, formulated in the previous section, is now solved to study the effect of an interface on the strain-gradient plasticity of a semi-infinite micro-slab. We consider two cases with initial position of the interface at $L/2$ and $L/4$, respectively. In the former, due to symmetry, the interface remains stationary during the deformation of the slab. In the latter case, however, the interface propagates with a finite speed so as to further reduce the thickness of the thinner region. In all our examples, in order to highlight the role of the interface on the overall plasticity of the slab, we calculate both the distribution of plastic strain field and the average stress-strain behavior in the slab.

For all our calculations we assume modulus of elasticity of bulk $E = 100$ GPa, Poisson's ratio of bulk $\nu = 0.3$, $K = 100$ MPa, $H = 20$ GPa, $k_0 = 0.08$ N/m, $h_0 = 10$ N/m, $b_0 + b_1 = -1$ N/m (Aifantis et al., 2006; Al-Rub, 2008). The Lamé constants λ and μ are obtained using the standard relations $\lambda = E\nu/\big((1 - 2\nu)(1 + \nu)\big)$ and $\mu = E/(2(1 + \nu))$. We define the average of a bulk field, say $f(y)$, as $\bar{f} = (1/L)\int_0^L f(y)\,dy$.

4.1. Interface at $y = L/2$

We assume the mean total strain $\bar{\epsilon}$ to remain non-negative. Moreover, in accordance with experimental observations (Aifantis et al., 2006), we will assume interface yielding to be always preceded by yielding in the bulk. Before the bulk starts to deform plastically, there exists a constant strain field in G given by $\epsilon = \Sigma/(\lambda + 2\mu)$, as calculated from $(30)_3$ with $\epsilon^p = 0$. The applied force Σ, at which yielding initiates, can be obtained by putting $\mathcal{F} = 0$ in (33) as $\Sigma_a = 2K/3\mathcal{A}$. The subscript a has been used to indicate the value of the variable at initial yielding of the bulk. In terms of strain, $\bar{\epsilon}_a = \epsilon_a = \Sigma_a/(\lambda + 2\mu)$. When $\Sigma > \Sigma_a$, or equivalently $\bar{\epsilon} > \bar{\epsilon}_a$, the plastic strain field evolves in the bulk (away from the interface). Assuming $\dot{\epsilon}^p > 0$, the PDE governing the evolution of plastic strain can then be obtained from (34) and (35) as

$$\frac{\partial^2\dot{\epsilon}^p}{\partial y^2} - \frac{1}{\ell^2}\dot{\epsilon}^p = -\frac{\mathcal{A}\dot{\Sigma}}{\ell^2(\mathcal{B} + \frac{2}{3}H)}, \tag{45}$$

Please cite this article as: A. Basak, A. Gupta, Influence of a mobile incoherent interface on the strain-gradient plasticity of a thin slab, International Journal of Solids and Structures (2016), http://dx.doi.org/10.1016/j.ijsolstr.2016.12.004

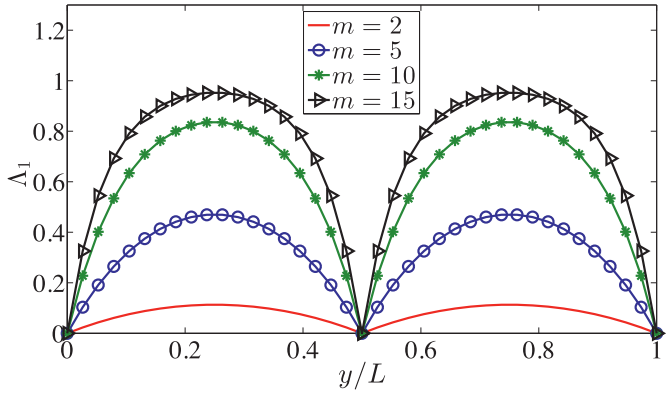

Fig. 3. Non-dimensional plastic strain-rate Λ_1, before interface has yielded, for various m when the interface is located at $y = L/2$.

where $\ell^2 = c/(3\mathcal{B}/2 + H)$ is an internal length scale associated with the inhomogeneity within the bulk (we assume $c > 0$). It is clear that incorporating a non-trivial ℓ in the theory is tantamount to bringing second-order effects in the plastic evolution. The length scale ℓ can also be seen as controlling the effective hardening of the solid due to inhomogeneous plastic deformation. It was interpreted as the length of dislocation pileup near the boundaries by Aifantis et al. (2006). As $\ell \to 0$, (45) leads to the classical plasticity solution of constant plastic strain in the entire slab. We will discuss more about ℓ in our subsequent discussion. Equations like (45) were first proposed by Aifantis (1984); 1987) in an attempt to introduce non-locality in plasticity theory. It should be emphasized that the appearance of the second-gradient term here is due to introduction of incompatibility in the yield function, as compared to being derived from a micro force balance (Gurtin and Anand, 2005; 2009). Eq. (45) can be solved, using boundary conditions (43) and $\dot{\epsilon}^p_+ = \dot{\epsilon}^p_- = 0$ (at $y = L/2$), to obtain plastic strain-rate field prior to interface yielding as

$$\dot{\epsilon}^p(y) = \frac{\mathcal{A}\dot{\Sigma}}{\mathcal{B} + \frac{2}{3}H}\Lambda_1(y), \tag{46}$$

where

$$\Lambda_1(y) = \begin{cases} 1 - \dfrac{\sinh(my/L) + \sinh(m/2 - my/L)}{\sinh(m/2)} & \text{if } 0 \le y \le L/2, \\ 1 - \dfrac{\sinh(my/L - m/2) + \sinh(m - my/L)}{\sinh(m/2)} & \text{if } L/2 \le y \le L, \end{cases} \tag{47}$$

is the non-dimensional plastic strain-rate and $m = L/\ell$. Fig. 3 plots Λ_1 for various m. For fixed L and increasing m, and hence decreasing ℓ, there are thinner boundary layers as well as increasing magnitudes of non-dimensional plastic strain-rates (bounded by 1). As the internal length scale ℓ approaches the thickness of the slab L, the amplitude of plastic strain-rate decreases making it difficult for the slab to deform plastically. In such a case the inhomogeneities (such as dislocation pileups) occupy a larger fraction of the slab. These conclusions are qualitatively in agreement with recently reported results of gradient plasticity predictions and 3D discrete dislocation dynamics simulations (Zhang and Aifantis, 2015; Zhang et al., 2014b). We can now establish an average stress-strain relation, prior to interface yielding, by first calculating the rate of average total strain using $(30)_3$,

$$\dot{\bar{\epsilon}} = \frac{\dot{\Sigma}}{\lambda + 2\mu} + \frac{2\mu}{L(\lambda + 2\mu)}\int_0^L \dot{\epsilon}^p dy, \tag{48}$$

then substituting plastic strain-rate from (46) into (48), and finally integrating the resulting expression with respect to time, as

$$\Sigma = \Sigma_a + \frac{(\mathcal{B} + \frac{2}{3}H)(\lambda + 2\mu)}{\mathcal{B} + \frac{2}{3}H + 2\mu\mathcal{A}\bar{\Lambda}_1}(\bar{\epsilon} - \bar{\epsilon}_a), \tag{49}$$

where $\bar{\Lambda}_1 = 1 - 4\tanh(m/4)/m$.

At the onset of interface yielding, since ϵ^p_+ and ϵ^p_- remain zero, relations (36)–(39) imply that both τ_e and e^p vanish identically. The interface of course remains stationary due to vanishing of the driving force. In order to calculate Σ at which interface yields, we substitute (37) in $\mathcal{G} = 0$, and evaluate plastic strains by integrating (46) with respect to time, to obtain

$$\Sigma_b = \Sigma_a + \frac{k_0}{2\ell_0 m_0 \mathcal{A}\tanh(m/4)}, \tag{50}$$

where we have introduced a new length scale $\ell_0^2 = c_0/(\mathcal{B} + \frac{2}{3}H)$ and a non-dimensional parameter $m_0 = \ell_0/\ell$. We use subscript b to indicate the value of the variable at the onset of interfacial yield. ℓ_0 characterizes the thickness of a region in the neighborhood of the interface where the interactions between bulk and interfacial plasticity remain concentrated. In particular, a smaller ℓ_0 will restrict the interfacial plastic flow to a narrower region in addition to increasing the value of Σ_b, for fixed ℓ. The parameter m_0, on the other hand, represents the fraction of boundary layer thickness at the interface as a result of interfacial yielding. We can obtain the average total strain at the onset of interface yielding, by using $\Sigma = \Sigma_b$ in (49), as

$$\bar{\epsilon}_b = \bar{\epsilon}_a + \frac{\mathcal{B} + \frac{2}{3}H + 2\mu\mathcal{A}\bar{\Lambda}_1}{(\lambda + 2\mu)(\mathcal{B} + \frac{2}{3}H)}(\Sigma_b - \Sigma_a). \tag{51}$$

So far we have investigated the plastic response of the slab before interface C has yielded. When Σ is increased beyond Σ_b there is a sudden transmission of plastic flow across the interface (Aifantis et al., 2006; Hosson et al., 2006; Morris et al., 2007). Followed by such strain burst, the plastic strains at the interface ϵ^p_+ and ϵ^p_- evolve. Since the interface is located at $L/2$, the symmetries in both geometry of the slab and external loading ensure that the response remains symmetric about the interface and, in particular, plastic strain field ϵ^p remains continuous across the interface. The interface therefore remains coherent at all times. The driving force in (36) also vanishes keeping the interface stationary. As a result we now solve (45), with boundary conditions provided by (42) and (43), to obtain

$$\dot{\epsilon}^p(y) = \frac{\mathcal{A}\dot{\Sigma}}{\mathcal{B} + \frac{2}{3}H}\Lambda_2(y), \tag{52}$$

where

$$\Lambda_2(y) = \begin{cases} 1 - \dfrac{h_0[\sinh(my/L) + \sinh(m/2 - my/L)] + 2m_0\ell_0(\mathcal{B} + \frac{2}{3}H)\cosh(m/2 - my/L)}{h_0\sinh(m/2) + 2m_0\ell_0(\mathcal{B} + \frac{2}{3}H)\cosh(m/2)} \\ \text{if } 0 \le y \le L/2 \text{ and} \\ 1 - \dfrac{h_0[\sinh(m - my/L) + \sinh(my/L - m/2)] + 2m_0\ell_0(\mathcal{B} + \frac{2}{3}H)\cosh(my/L - m/2)}{h_0\sinh(m/2) + 2m_0\ell_0(\mathcal{B} + \frac{2}{3}H)\cosh(m/2)} \\ \text{if } L/2 \le y \le L \end{cases} \tag{53}$$

Please cite this article as: A. Basak, A. Gupta, Influence of a mobile incoherent interface on the strain-gradient plasticity of a thin slab, International Journal of Solids and Structures (2016), http://dx.doi.org/10.1016/j.ijsolstr.2016.12.004

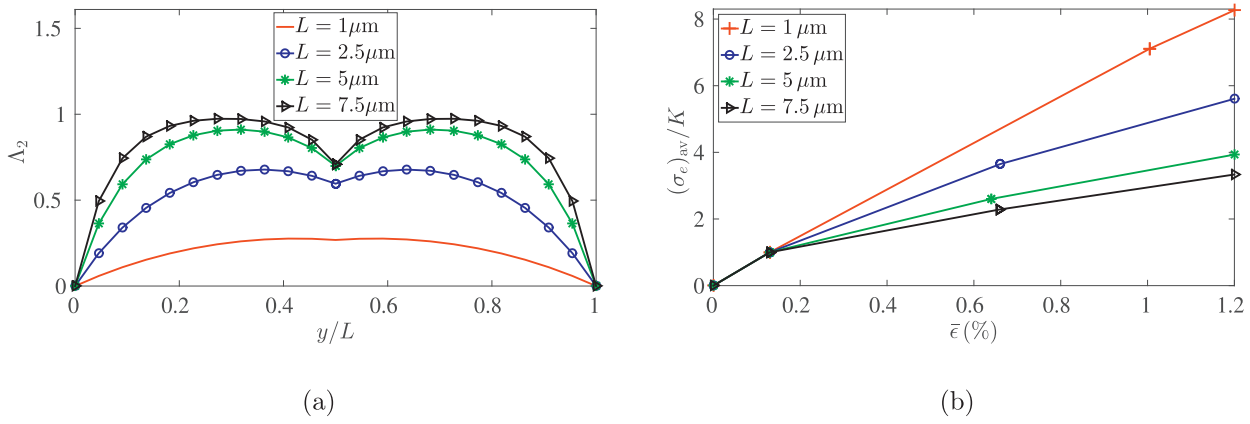

Fig. 4. (a) Non-dimensional plastic strain-rate Λ_2, post interface yield, and (b) the average effective stress-strain response for various L. We take $\ell = 500$ nm and $\ell_0 = 10$ nm.

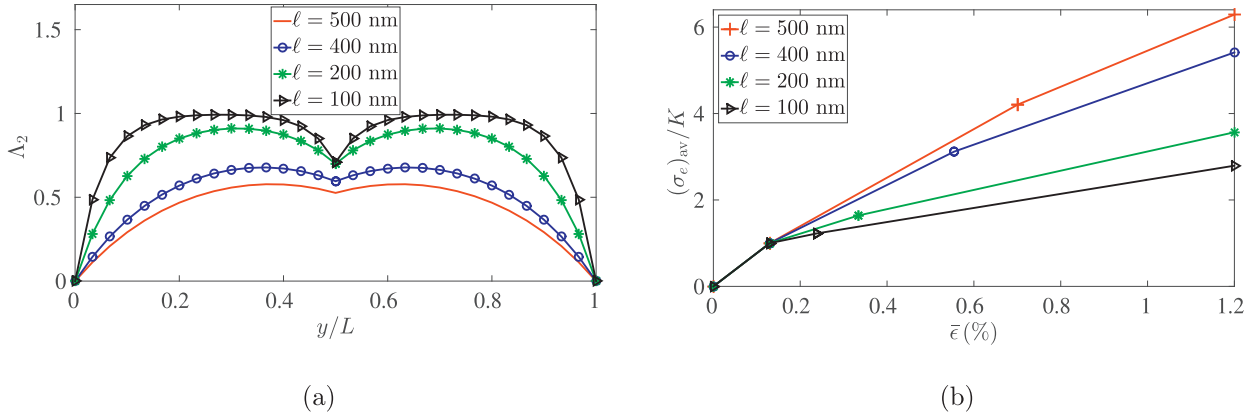

Fig. 5. (a) Non-dimensional plastic strain-rate Λ_2, post interface yield, and (b) the average effective stress-strain response for various ℓ. We take $L = 2\,\mu$m and $\ell_0 = 10$ nm.

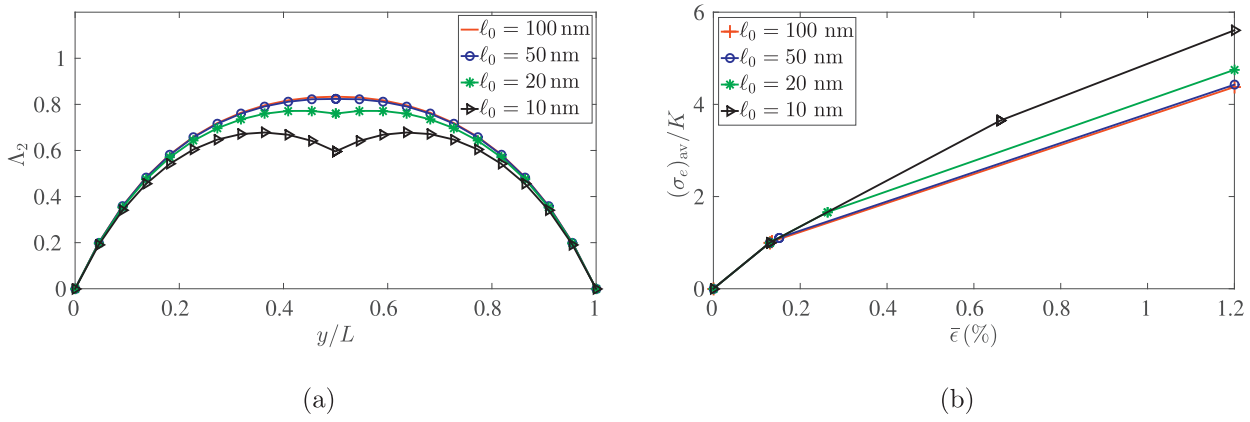

Fig. 6. (a) Non-dimensional plastic strain-rate Λ_2, post interface yield, and (b) the average effective stress-strain response for various ℓ_0. We take $\ell = 500$ nm and $L = 2.5\,\mu$m.

is the non-dimensional plastic strain-rate post interface yielding. Recalling that there are three distinct length scales, L, ℓ, and ℓ_0 in our theory, we plot Λ_2 with variations in each of these, while keeping others fixed, in Figs. 4(a), 5(a), and 6(a). According to Fig. 4(a), for fixed boundary layer width (i.e., ℓ) and fixed effective interface thickness (i.e., ℓ_0), the thinner slabs are less amenable to plastic deformation and inhomogeneities (such as dislocation pile-ups), represented by plastic strain gradients, cover larger fraction of the slab. For thicker slabs the strain gradients are concentrated in small neighborhoods around internal and external boundaries. In Fig. 5(a) we observe that, for fixed L and ℓ_0, an increase in ℓ reduces the amplitude of the plastic strain while spreading inhomogeneity distribution over a larger fraction of the slab. Our predictions are in close qualitative agreement with similar behavior reported in recently obtained gradient plasticity results and discrete dislocation dynamics simulations (Zhang and Aifantis, 2015; Zhang et al., 2014b) (see also Aifantis and Willis, 2005; Aifantis et al., 2006; Polizzotto, 2009). It should be however noted that the interfacial length scale ℓ_0 is absent from the gradient plasticity theory used in the cited papers. The following discussion with respect to variations in ℓ_0, therefore, has no direct analogy for comparison with that work. According to Fig. 6(a), where we have fixed L and ℓ, with an increasing ℓ_0 the interfacial plastic flow occurs in a more diffused manner resulting in a smoother distribution of plastic strain over the slab. On the other hand, if ℓ_0 decreases below 10 nm, interface yielding becomes increasingly difficult, possibly due

Please cite this article as: A. Basak, A. Gupta, Influence of a mobile incoherent interface on the strain-gradient plasticity of a thin slab, International Journal of Solids and Structures (2016), http://dx.doi.org/10.1016/j.ijsolstr.2016.12.004

to vanishing of space for intergranular dislocation transfer. The interface will then behave as a microscopically hard boundary between the two bulk regions. We also note that, although our interpretation for ℓ_0 is analogous to that given earlier in the works of Fredriksson and Gudmundson (2007), Fredriksson and Gudmundson (2005), Gudmundson (2004) and Al-Rub (2008), the origins of such a length scale in our theory is fundamentally different from theirs.

The average stress-strain relationship, post interface yield, can be obtained by substituting (52) into (48) and then integrating with respect to time. Collectively, recalling previous results, we can write the stress-strain relations for the slab with a stationary interface at $L/2$ as

$$\Sigma = \begin{cases} (\lambda+2\mu)\bar{\epsilon} & \text{if } \bar{\epsilon} \le \bar{\epsilon}_a, \\ \Sigma_a + \dfrac{(\mathcal{B}+\frac{2}{3}H)(\lambda+2\mu)}{\mathcal{B}+\frac{2}{3}H+2\mu\mathcal{A}\bar{\Lambda}_1}(\bar{\epsilon}-\bar{\epsilon}_a) & \text{if } \bar{\epsilon}_a \le \bar{\epsilon} \le \bar{\epsilon}_b, \\ \Sigma_b + \dfrac{(\mathcal{B}+\frac{2}{3}H)(\lambda+2\mu)}{\mathcal{B}+\frac{2}{3}H+2\mu\mathcal{A}\bar{\Lambda}_2}(\bar{\epsilon}-\bar{\epsilon}_b) & \text{if } \bar{\epsilon} \ge \bar{\epsilon}_b, \end{cases} \tag{54}$$

where

$$\bar{\Lambda}_2 = 1 - \left(\frac{4}{m}\right)\frac{h_0(\cosh(m/2)-1)+m_0\ell_0(\mathcal{B}+\frac{2}{3}H)\sinh(m/2)}{h_0\sinh(m/2)+2m_0\ell_0(\mathcal{B}+\frac{2}{3}H)\cosh(m/2)}. \tag{55}$$

The average stress-strain plots are shown in Figs. 4(b), 5(b), and 6(b) for various choice of parameters. In fact, we have given plots for the average effective stress, defined as $(\sigma_e)_{\text{av}} = 3|\mathcal{A}\,\Sigma - \mathcal{B}\,\bar{\epsilon}^p|/2$. In Fig. 4(b) the first kinks appear at around $\bar{\epsilon} = 0.13\%$, indicating yielding of the bulk. The second kink, which appears at different strain values for different slab width (keeping ℓ and ℓ_0 fixed), represents a strain burst and subsequent yielding at the interface. The kinks produce a 'knee' like feature in the stress-strain diagrams. With decreasing slab thickness the effective hardening of the slab is clearly shown to be enhanced, as has been observed in various indentation tests (Aifantis et al., 2006; Hosson et al., 2006). The two kinks in Fig. 5(b) again indicate yielding of the bulk and the interface, respectively. With an increasing width of boundary layers (and therefore of pileups), while keeping L and ℓ_0 fixed, there is a significant increase in the hardening as well in the magnitude of critical average strain required for the interface to yield. Our predictions for stress-strain curves for varying L and ℓ are generally in agreement with the existing literature (Aifantis and Willis, 2005; Aifantis et al., 2006; Aifantis and Willis, 2004; Polizzotto, 2009). These works however use a gradient theory which does not include ℓ_0 and therefore have no comparable results to our following discussion on the variation of stress-strain curves with respect to ℓ_0 (see also Fredriksson and Gudmundson, 2007; 2005; Gudmundson, 2004; Al-Rub, 2008). In Fig. 6(b) we plot the stress-strain relationship with varying ℓ_0, keeping L and ℓ fixed. The slope of the stress-strain curve remains identical for all the cases until the interface yields. Moreover, for large values of ℓ_0, the bulk and interface yield points are found to be almost coinciding with each other. This is expected since, with increase in ℓ_0, the interface would become weaker and yield sooner, as can be verified from (50) and (51). We also note that the effective hardening of the slab increases with decreasing ℓ_0. Finally, we remark that the typical values of ℓ and ℓ_0, that we have used in the above results, are inspired from Aifantis et al. (2006), where they were motivated experimentally, and from Fredriksson and Gudmundson (2005), where they were motivated from the strength behavior of thin films, respectively.

4.2. Interface initially at $y = L/4$

We now consider the interface C to be initially located at $y = L/4$ such that region G_2 is three times thicker than G_1. Since we have already studied the role of various length scales on the plasticity of the slab, we will fix $L = 2\,\mu$m, $\ell = 500$ nm, and $\ell_0 = 10$ nm. Contrary to the case when C was initially at $L/2$, the interface will now become incoherent soon after it yields and acquire a finite speed of propagation. As a result, our interest here is to study the effect of mobility of the interface on the average plastic behavior of the slab. We will also study the effect of varying average strain-rate while keeping mobility fixed. As was the case in the last section, we will assume interface to yield after bulk has yielded. However, we will assume the thinner portion of the slab, i.e., G_1, to remain elastic throughout, even after the interface has yielded and started to propagate, i.e., $\epsilon^p = 0$ in $0 \le y < \xi$ and $\epsilon^p_- = 0$. This is justified since, after using (43) and (45) to solve for plastic strain post bulk yielding, we note that the amplitude of plastic strain in G_1 remains almost an order of magnitude smaller than that in G_2. Moreover it is easy to estimate, from (24) and (36), that the interface will move in a direction so as to further reduce the size of G_1 allowing us to retain the assumption of vanishing plastic strain in G_1 when the interface has yielded and is propagating with a finite speed.

The stress and the average strain at which G_2 yields can be evaluated, using $(30)_3$ and (33), as $\Sigma_c = 2K/3\mathcal{A}$ and $\bar{\epsilon}_c = \Sigma_c/(\lambda+2\mu)$, where we have used the subscript c to denote quantities at the initial yielding of G_2. The region G_2 deforms plastically for $\Sigma \ge \Sigma_c$. However, until C_+ yields, the interface behaves as a microscopically hard boundary, i.e., $\epsilon^p_+ = 0$. This in conjunction with (43) can be used to solve the PDE (45) to obtain the plastic strain-rate in G_2, before interface yields, as

$$\dot{\epsilon}^p(y) = \frac{\mathcal{A}\dot{\Sigma}}{\mathcal{B}+\frac{2}{3}H}\Lambda_3(y) \quad \text{for } L/4 \le y \le L, \tag{56}$$

where

$$\Lambda_3(y) = 1 - \frac{\sinh(my/L - m/4)+\sinh(m-my/L)}{\sinh(3m/4)}. \tag{57}$$

Substituting (56) into (48), and then integrating with respect to time, we can establish the average stress-strain relationship in the slab prior to interface yielding as

$$\Sigma = \Sigma_c + \frac{(\lambda+2\mu)(\mathcal{B}+\frac{2}{3}H)}{\mathcal{B}+\frac{2}{3}H+2\mu\mathcal{A}\bar{\Lambda}_3}(\bar{\epsilon}-\bar{\epsilon}_c), \tag{58}$$

where $\bar{\Lambda}_3 = (3/4) - (2\tanh(3m/8)/m)$. The applied force Σ at which interface C_+ yields can be obtained, using (37) in $\mathcal{G} = 0$, as

$$\Sigma_d = \Sigma_c + \frac{k_0\coth(3m/8)}{\ell_0 m_0 \mathcal{A}}. \tag{59}$$

The subscript d is used to indicate the value of quantities at the initial yielding of C_+. The critical force in (59) can be substituted in (58) to calculate the average strain $\bar{\epsilon}_d$ at which C_+ yields,

$$\bar{\epsilon}_d = \bar{\epsilon}_c + \frac{\mathcal{B}+\frac{2}{3}H+2\mu\mathcal{A}\bar{\Lambda}_3}{(\lambda+2\mu)(\mathcal{B}+\frac{2}{3}H)}(\Sigma_d - \Sigma_c). \tag{60}$$

Once the average strain $\bar{\epsilon}$ exceeds $\bar{\epsilon}_d$, plastic strain ϵ^p_+ starts to evolve. The strain ϵ^p_- however remains zero. This introduces incoherency at the interface. The driving force in (36) also acquires a non-trivial value forcing the interface to move with a finite speed as governed by the kinetic law in (24). The PDE (45) is now solved under these considerations. Let $y = \xi(t)$ be the instantaneous position of the interface. Using boundary condition (43), the plastic strain-rate in G_2 can be obtained as

$$\dot{\epsilon}^p(y) = \frac{\mathcal{A}\dot{\Sigma}}{\mathcal{B}+\frac{2}{3}H}\Lambda_4(y) + \dot{\epsilon}^p_+\Lambda_5(y) \quad \text{in } \xi(t) \le y \le L, \tag{61}$$

Please cite this article as: A. Basak, A. Gupta, Influence of a mobile incoherent interface on the strain-gradient plasticity of a thin slab, International Journal of Solids and Structures (2016), http://dx.doi.org/10.1016/j.ijsolstr.2016.12.004

where

$$\Lambda_4(y) = 1 - \frac{\sinh(my/L - m\xi/L) + \sinh(m - my/L)}{\sinh(m - m\xi/L)} \quad \text{and}$$
$$\Lambda_5(y) = \frac{\sinh(m - my/L)}{\sinh(m - m\xi/L)}. \tag{62}$$

In (61) $\dot{\epsilon}^p_+$ is to be determined using the governing equations for interfacial plasticity, given by (40) and (41), in addition to the kinetic law (24). It is not possible to solve the problem analytically any further. Towards this end, we will discretize the time derivatives using a forward finite difference scheme. For instance, $\dot{\epsilon}^p_+$ is discretized as $\Delta\epsilon^p_+/\Delta t$, where $\Delta\epsilon^p_+ = (\epsilon^p_+)_{n+1} - (\epsilon^p_+)_n$, $\Delta t = t_{n+1} - t_n$, and the suffix $n = 0, 1, 2, \ldots$ denotes the index of time instant. The time t_0 denotes the instance when C_+ initially yields. Differentiating (61) with respect to y and discretizing in time, followed by evaluating it at the interface, we obtain

$$\left(\frac{\partial \epsilon^p}{\partial y}\bigg|_+\right)_{n+1} = \left(\frac{\partial \epsilon^p}{\partial y}\bigg|_+\right)_n + \frac{m\mathcal{A}Z\,\Delta\Sigma}{L(\mathcal{B} + \frac{2}{3}H)} - \frac{m}{L}\Delta\epsilon^p_+ \coth(m - m\xi_n/L) \quad \text{and} \tag{63}$$

$$\left(\frac{\partial^2 \epsilon^p}{\partial y^2}\bigg|_+\right)_{n+1} = \left(\frac{\partial^2 \epsilon^p}{\partial y^2}\bigg|_+\right)_n - \frac{m^2\mathcal{A}\Delta\Sigma}{L^2(\mathcal{B} + \frac{2}{3}H)} + \frac{m^2\Delta\epsilon^p_+}{L^2}, \tag{64}$$

where $Z = \tanh(m/2 - m\xi_n/2L)$. The interfacial plastic strain at $(n+1)_{th}$ time step, $(\epsilon^p_+)_{n+1}$, can be evaluated from $(40)_1$, after using (7) and (41), as

$$(\epsilon^p_+)_{n+1} = (\epsilon^p_+)_n + \frac{\mathcal{A}\Delta\Sigma}{(\mathcal{B} + \frac{2}{3}H)}\frac{Q_2}{Q_1} + \frac{Q_3}{Q_1}, \tag{65}$$

where

$$Q_1 = 1 - \frac{mV_n\Delta t}{L}\coth(m - m\xi_n/L) - \frac{c_0 m\,T_n}{Lh_{\text{eff}}}\left(\frac{mV_n\Delta t}{L} - \coth(m - m\xi_n/L)\right), \tag{66}$$

$$Q_2 = \frac{c_0 m\,T_n}{Lh_{\text{eff}}}(Z - mV_n\Delta t/L) - \frac{V_n mZ\Delta t}{L}, \tag{67}$$

$$Q_3 = \frac{c_0\,T_n V_n \Delta t}{h_{\text{eff}}}\left(\frac{\partial^2 \epsilon^p}{\partial y^2}\bigg|_+\right)_n - V_n\Delta t\left(\frac{\partial \epsilon^p}{\partial y}\bigg|_+\right)_n, \tag{68}$$

$T_n = -\text{sign}((b_0 + b_1)(\epsilon^p_+ - \epsilon^p_-)_n)$, and V_n is the interface velocity at n_{th} time step. In deriving (65) we have also used (63) and (64). In order to obtain a discrete version of the average stress-strain relationship we first write the plastic strain in the bulk, using (65) in the time discretized form of (61), as

$$\epsilon^p_{n+1} = \epsilon^p_n + \frac{\mathcal{A}(\Sigma_{n+1} - \Sigma_n)}{\mathcal{B} + \frac{2}{3}H}\left(\Lambda_4 + \frac{Q_2\Lambda_5}{Q_1}\right) + \frac{Q_3\Lambda_5}{Q_1} \quad \text{in } \xi(t) \le y \le L. \tag{69}$$

Next, we recall $(30)_3$ to write the rate of average strain in the form

$$\dot{\bar{\epsilon}} = \frac{\dot{\Sigma}}{\lambda + 2\mu} + \frac{2\mu}{L(\lambda + 2\mu)}\int_\xi^L \dot{\epsilon}^p\,dy - \frac{2\mu V}{L(\lambda + 2\mu)}\epsilon^p_+, \tag{70}$$

where we have used the Leibniz integral rule and $V = \dot{\xi}$. Finally, discretizing (70) in time employing the explicit scheme, and using (69), we get the average stress-strain relation:

$$\Sigma_{n+1} = \Sigma_n + \frac{(\lambda + 2\mu)(\mathcal{B} + \frac{2}{3}H)}{\mathcal{B} + \frac{2}{3}H + 2\mu\mathcal{A}Q_4} \times \left(\bar{\epsilon}_{n+1} - \bar{\epsilon}_n - \frac{2\mu}{\lambda + 2\mu}\left(Q_5 - V_n(\epsilon^p_+)_n\frac{\Delta t}{L}\right)\right), \tag{71}$$

which holds after interface has yielded, i.e., when $\bar{\epsilon} > \bar{\epsilon}_d$. The average stress-strain relation before interface yield, but after bulk has yielded, is given by (58). Here

$$Q_4 = 1 - \frac{\xi}{L} + \frac{Z}{m}\left(\frac{Q_2}{Q_1} - 2\right) \quad \text{and} \quad Q_5 = \frac{Q_3 Z}{Q_1 m}. \tag{72}$$

We can substitute (71) in (69) and (65) to derive the time discretized expressions for plastic strain in the slab and the plastic strain at C_+, respectively. In particular, for average plastic strain in the slab we obtain

$$\bar{\epsilon}^p_{n+1} = \bar{\epsilon}^p_n + \frac{\mathcal{A}(\Sigma_{n+1} - \Sigma_n)}{\mathcal{B} + \frac{2}{3}H}Q_4 + Q_5 - \frac{V_n(\epsilon^p_+)_n\Delta t}{L} \qquad \text{if } \bar{\epsilon} \ge \bar{\epsilon}_b. \tag{73}$$

We will use this expression to compute the average effective stress in the slab. On the other hand, the updated position of the interface is calculated using $\xi_{n+1} = \xi_n + \Delta t V_n$.

In rest of this section we will investigate the nature of our solutions by plotting the evolution of interface position and interfacial plastic strain with time in addition to plotting the average effective stress-strain response in the slab. We will study the variations in these plots for various values of interface mobility and the average strain-rate. An increase in mobility can be physically interpreted as increase in the temperature of the system (Winning et al., 2001). For all our calculations we assume $(\epsilon^p_+)_0 = 10^{-6}$. According to Fig. 7(a), as expected, interface propagates faster with increasing mobility. There is no interface movement until it has yielded. It is also clear from the plots that the interfacial speed is sensitive to even small variations in the mobility; in fact, above certain values of mobility, it can move at very high speeds. We have not reported data after a point when interface is close to the external boundary. At this point the interface might start to interact with the boundary and can have a different response than what has been formulated in our work. With increasing mobility, the plastic strain accumulated at the interface also increases, as has been shown in Fig. 7(b). Therefore, one can relate speed of the interface motion with plastic strain accumulation at the interface. A higher value of the latter also signifies higher incoherency at the interface, which is equivalent to, e.g., high density of interface dislocations. The effect of mobility on the average stress-strain response of the slab is shown in 7(c). The stress-strain responses are identical prior to interface yielding, but differ significantly afterwards. The average stress-strain response is increasingly nonlinear, with a well defined maxima, for higher values of interfacial mobility. The interface propagation relaxes the stress in the slab, more so for higher mobilities. This is evident in the softening response soon after interface yielding. In other words, a fast moving interface would relax the stress more rapidly than a slower one. Such softening in polycrystalline materials, with average grain size of microns, sub-microns, and nano scales, has been reported widely in the experimental literature (Chen and Gottstein, 1988; Morris et al., 2007; Legros et al., 2008).

To obtain a different perspective from our formulation, we now consider the slab deformation to be instead controlled by prescribing displacements on the free boundary. In such a process, we fix the value of the average strain-rate $\dot{\bar{\epsilon}}$ and calculate the load accordingly. We again plot interface position, plastic strain accumulation, and stress-strain response of the slab for various values of the average strain-rate. The mobility value is kept constant. It is

Please cite this article as: A. Basak, A. Gupta, Influence of a mobile incoherent interface on the strain-gradient plasticity of a thin slab, International Journal of Solids and Structures (2016), http://dx.doi.org/10.1016/j.ijsolstr.2016.12.004

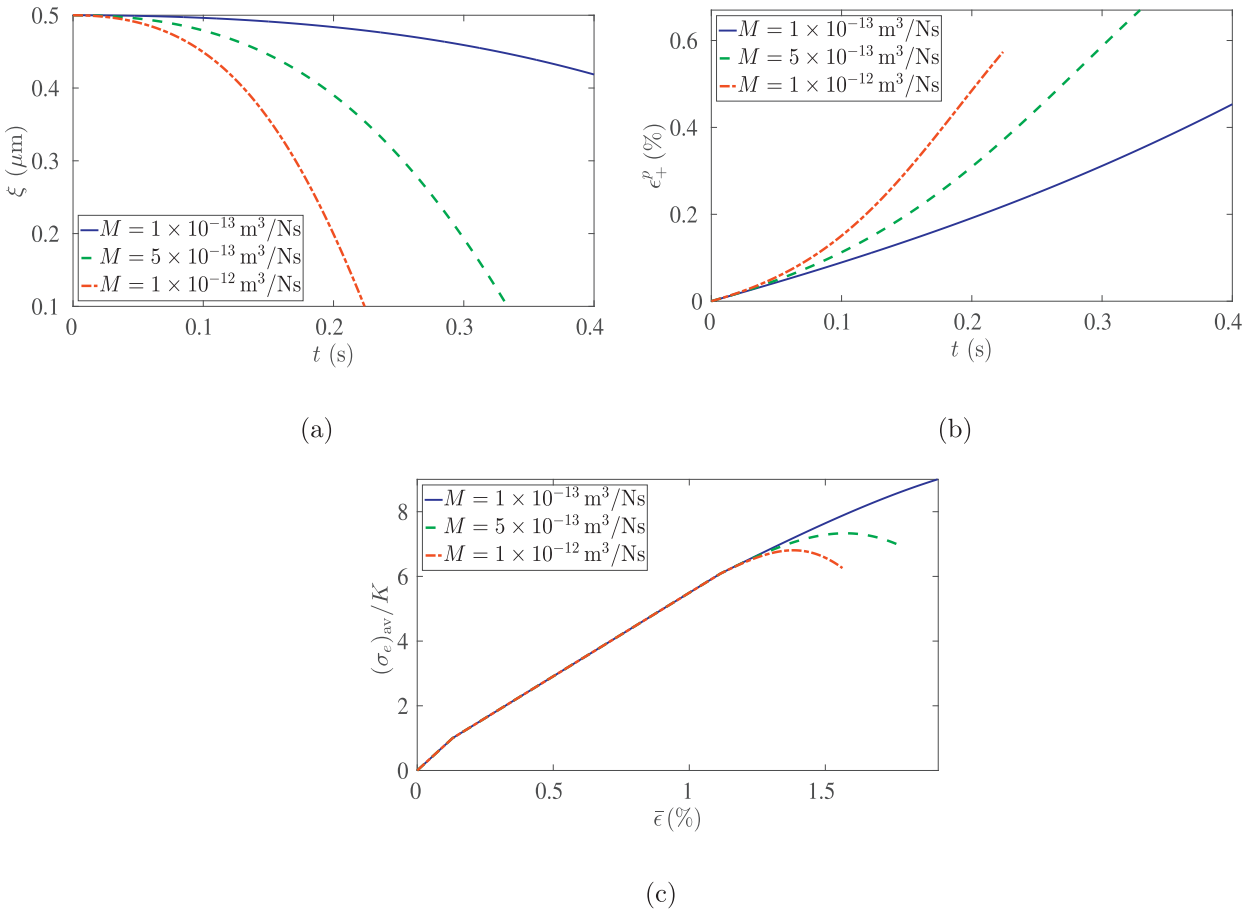

Fig. 7. Plots for (a) position of the interface with time, (b) plastic strain at the interface with time, and (c) average effective stress-strain response of the slab for varying interfacial mobility. We have used $L = 2\,\mu$m, $\ell = 500$ nm, $\ell_0 = 10$ nm, $\Delta\bar{\epsilon} = 2 \times 10^{-9}$, and $\Delta t = 10^{-7}$ s.

evident from Fig. 8(a) and (b) that, as we consider higher values of average strain-rate, the plastic strain accumulation at the interface increases and the interface moves at a faster speed. The motion of the interface relaxes the stress in the slab and introduces strain softening in the solid. According to Fig. 8(c), with increasing strain-rate, stress relaxation gets delayed and the maximum stress is attained at higher average strains. A qualitatively similar strain-rate softening effect in polycrystalline materials has been reported in an earlier experimental study (Chen and Gottstein, 1988). We note that both interfacial speed and plastic accumulation are raised for increasing average strain-rate as well as increasing mobility. On the other hand, a more softening behavior is predicted for larger mobility but smaller average strain-rate. This is reasonable since larger mobility leads to greater plastic strain accumulation, but at the same time also to a faster transmission of plastic strain to the neighboring grain.

It is clearly seen from the results of last two subsections that, under the action of external load, the interface will remain stationary at all times only if it is situated in the middle of the slab, at $y = L/2$. Otherwise, it will continue to move until it escapes the slab while travelling through the thinner region. This makes the center position unstable, in a sense that a slightest perturbation from the center would lead the interface to move away towards the free surface. Such behavior is a consequence of the inherent symmetry of our material model (across the interface) and loading conditions, including isotropic plastic behavior and isotropic interfacial energy. Any deviations from the symmetry and isotropy, for instance by considering orientation dependent interfacial energies and heterophase interfaces, would resolve this anomalous conclusion from our theory.

5. Conclusions

We have developed a thermodynamically consistent framework of strain-gradient plasticity in isotropic solids with mobile interfaces. The strain gradients have been introduced in the yield functions as suitable measures of material inhomogeneity both in the bulk and at the interface. We have not considered any higher order stress fields in our theory (such as those used by Fleck and Hutchinson), neither have we employed any form of microforce balance laws (in contrast to the work by Gurtin and Anand). Associative plasticity flow rules have been proposed such that they remain coupled to interface kinetics. This provides us with an appropriate setting to pursue an analytical investigation on the nature of the overall plastic deformation in a semi-infinite thin slab, under tensile loading, with a propagating planar interface. In particular, we have studied the effect of varying length scales, two of which were internal, on the plastic strain distribution and the average effective stress-strain response of the slab. The two internal length scales were found to characterize the width of boundary layers and interface layer where most of the plastic inhomogeneity was accommodated. We also observed, for instance, that decreasing the slab thickness, or increasing the internal length scale associated with the bulk, or decreasing the internal length scale associated with the interface, results in an increase of the effective hardening of the slab. Moreover, allowing the interface to yield independently of the bulk, we noticed stress relaxation in the slab through transmission of bulk plastic strain across the interface. On the other hand, once the interface became mobile, it led to strain softening in the solid, which became prominent with increasing mobility, and a rate-dependent stress-strain response, even when

Please cite this article as: A. Basak, A. Gupta, Influence of a mobile incoherent interface on the strain-gradient plasticity of a thin slab, International Journal of Solids and Structures (2016), http://dx.doi.org/10.1016/j.ijsolstr.2016.12.004

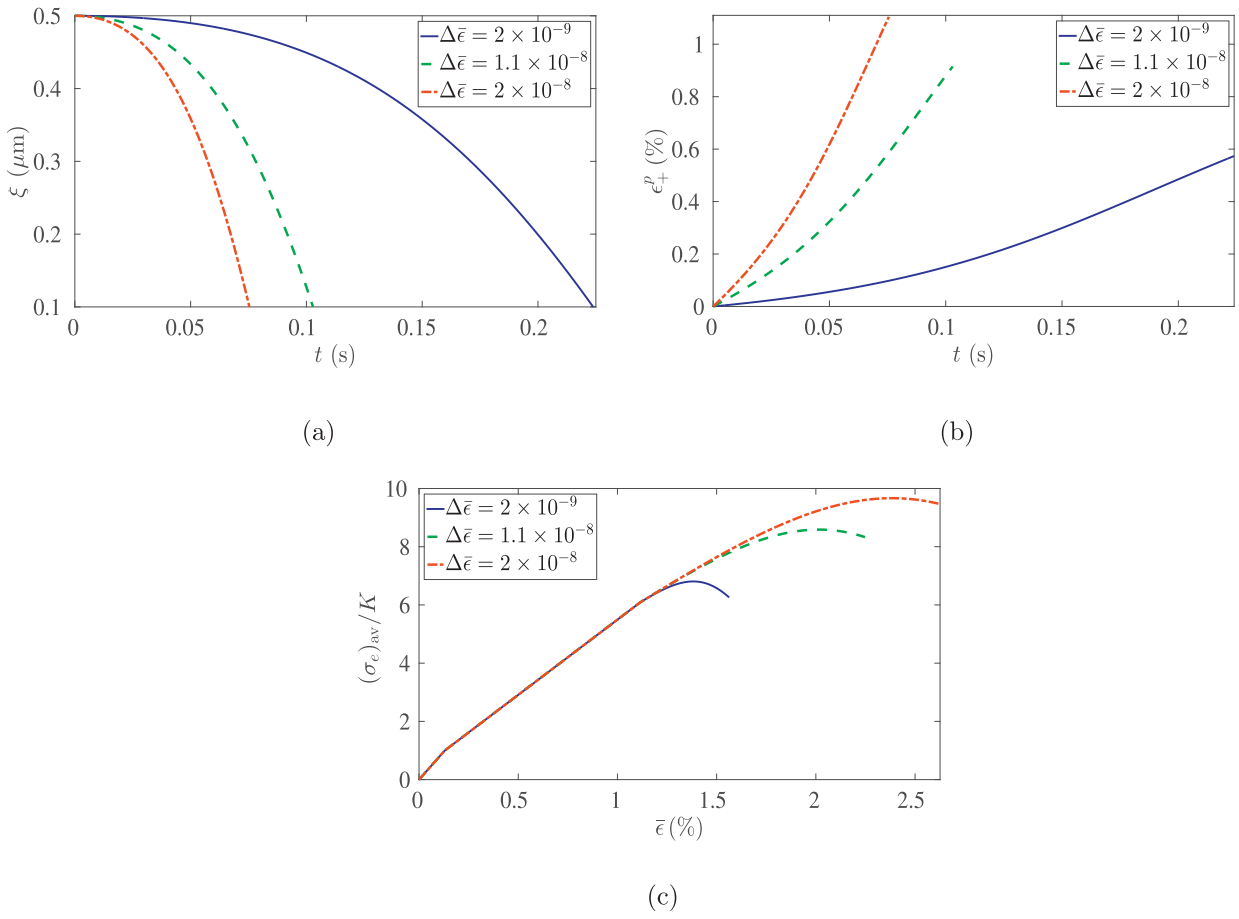

Fig. 8. Plots for (a) position of the interface with time, (b) plastic strain at the interface with time, and (c) average effective stress-strain response of the slab with varying average strain-rate. We have used $L = 2\,\mu$m, $\ell = 500$ nm, $\ell_0 = 10$ nm, $M = 10^{-12}$ m^3/Ns, and $\Delta t = 10^{-7}$ s.

the underlying plasticity was assumed to be rate-independent. The theory developed in the present work can be readily adapted to understand the role of mobile phase-transformation fronts on the overall plasticity of a multi-phase solid. On the other hand, the effect of junctions can be incorporated so to realistically model the microstructure of polycrystalline materials. The relevant theory in two-dimensions has already been presented elsewhere (Basak and Gupta, 2016).

References

Acharya, A., Bassani, J.L., 1996. On non-local flow theories that preserve the classical structure of incremental boundary value problems. In: Pineau, A., Zaoui, A. (Eds.), IUTAM Symposium on Micromechanics of Plasticity and Damage of Multiphase Materials. Kluwer Academic Publishers, Dordrecht, pp. 3–9.
Aifantis, E.C., 1984. On the microstructural origin of certain inelastic models. J. Eng. Mater. Technol. 106, 326–330.
Aifantis, E.C., 1987. The physics of plastic deformation. Int. J. Plast. 3, 211–247.
Aifantis, K.E., Soer, W.A., Hosson, J.T.M.D., Willis, J.R., 2006. Interfaces within strain gradient plasticity: theory and experiments. Acta Mater. 54, 5077–5085.
Aifantis, K.E., Willis, J.R., 2004. Interfacial jump conditions in strain-gradient plasticity and relations of Hall-Petch type. In: Kounadis, A., Providakis, C., Exadaktylos, G. (Eds.), Proceedings of the Seventh National Congress on Mechanics, vol. II, Chania, Greece, pp. 372–377.
Aifantis, K.E., Willis, J.R., 2005. The role of interfaces in enhancing the yield strength of composites and polycrystals. J. Mech. Phys. Solids 53, 1047–1070.
Aifantis, K.E., Willis, J.R., 2006. Scale effects induced by strain-gradient plasticity and interfacial resistance in periodic and randomly heterogeneous media. Mech. Mater. 38, 702–716.
Al-Rub, R.K.A., 2008. Interfacial gradient plasticity governs scale-dependent yield strength and strain hardening rates in micro/nano structured metals. Int. J. Plast. 24, 1277–1306.
Anand, L., Gurtin, M.E., Lele, S.P., Gething, C., 2005. A one-dimensional theory of strain-gradient plasticity: formulation, analysis, numerical results. J. Mech. Phys. Solids 53, 1789–1826.
Ashby, M.F., 1970. The deformation of plastically non-homogeneous materials. Philos. Mag. 21, 399–424.
Balint, D.S., Deshpande, V.S., Needleman, A., der Giessen, E.V., 2008. Discrete dislocation plasticity analysis of the grain size dependence of the flow strength of polycrystals. Int. J. Plast. 24, 2149–2172.
Basak, A., Gupta, A., 2015a. Simultaneous grain boundary motion, grain rotation, and sliding in a tricrystal. Mech. Mater. 90, 229–242.
Basak, A., Gupta, A., 2015b. A three-dimensional study of coupled grain boundary motion with junctions. Proc. R. Soc. London A 471, 20150127.
Basak, A., Gupta, A., 2016. Plasticity in multi-phase solids with incoherent interfaces and junctions. Continuum Mech. Thermodyn. 28, 423–442.
Bassani, J.L., 2001. Incompatibility and a simple gradient theory of plasticity. J. Mech. Phys. Solids 49, 1983–1996.
Boley, B.A., Weiner, J.H., 1997. Theory of Thermal Stresses. Dover, New York.
Cermelli, P., Gurtin, M.E., 1994. The dynamics of solid-solid phase transitions 2. Incoherent interfaces. Arch. Ration. Mech. Anal. 127, 41–99.
Chen, S., Gottstein, G., 1988. Strain softening, grain boundary migration and dynamic recrystallization of Ni during high temperature low cycle fatigue. Acta Metall. 36, 3093–3101.
Fleck, N.A., Hutchinson, J.W., 1997. Strain gradient plasticity. Adv. Appl. Mech. 33, 295–362.
Fleck, N.A., Hutchinson, J.W., 2001. A reformulation of strain gradient plasticity. J. Mech. Phys. Solids 49, 2245–2271.
Fleck, N.A., Muller, G.M., Ashby, M.F., Hutchinson, J.W., 1994. Strain gradient plasticity: theory and experiment. Acta Metall. Mater. 42, 475–487.
Fleck, N.A., Willis, J.R., 2009. A mathematical basis for strain-gradient plasticity theory-Part I: scalar plastic multiplier. J. Mech. Phys. Solids 57, 161–177.
Fredriksson, P., Gudmundson, P., 2005. Size-dependent yield strength of thin films. Int. J. Plast. 21, 1834–1854.
Fredriksson, P., Gudmundson, P., 2007. Modelling of the interface between a thin film and a substrate within a strain gradient plasticity framework. J. Mech. Phys. Solids 55, 939–955.
Fredriksson, P., Gudmundson, P., Mikkelsen, L.P., 2009. Finite element implementation and numerical issues of strain gradient plasticity with application to metal matrix composites. Int. J. Solids Struct. 46, 3977–3987.
Gao, H., Huang, Y., Nix, W.D., Hutchinson, J.W., 1999. Mechanism-based strain gradient plasticity – I. Theory. J. Mech. Phys. Solids 47, 1239–1263.

Please cite this article as: A. Basak, A. Gupta, Influence of a mobile incoherent interface on the strain-gradient plasticity of a thin slab, International Journal of Solids and Structures (2016), http://dx.doi.org/10.1016/j.ijsolstr.2016.12.004

Gorkaya, T., Molodov, K.D., Molodov, D.A., Gottstein, G., 2011. Concurrent grain boundary motion and grain rotation under an applied stress. Acta Mater. 59, 5674–5680.
Gourdet, S., Montheillet, F., 2002. Effects of dynamic grain boundary migration during the hot compression of high stacking fault energy metals. Acta Mater. 50, 2801–2812.
Gudmundson, P., 2004. A unified treatment of strain gradient plasticity. J. Mech. Phys. Solids 52, 1379–1406.
Gupta, A., Steigmann, D.J., 2012. Plastic flow in solids with interfaces. Math. Methods Appl. Sci. 35, 1799–1824.
Gurtin, M.E., Anand, L., 2005. A theory of strain-gradient plasticity for isotropic, plastically irrotational materials. part I: small deformations. J. Mech. Phys. Solids 53, 1624–1649.
Gurtin, M.E., Anand, L., 2009. Thermodynamics applied to gradient theories involving the accumulated plastic strain: the theories of Aifantis and Fleck and Hutchinson and their generalization. J. Mech. Phys. Solids 57, 405–421.
Gurtin, M.E., Jabbour, M.E., 2002. Interface evolution in three dimensions with curvature-dependent energy and surface diffusion: interface-controlled evolution, phase transitions, epitaxial growth of elastic films. Arch. Ration. Mech. Anal. 163, 171–208.
Hosson, J.T.M.D., Soer, W.A., Minor, A.M., Shan, Z., Stach, E.A., Asif, S.A.S., Warren, O.L., 2006. In situ TEM nanoindentation and dislocation-grain boundary interactions: a tribute to David Brandon. J. Mater. Sci. 41, 7704–7719.
Huang, Y., Gao, H., Nix, W.D., Hutchinson, J.W., 2000. Mechanism-based strain gradient plasticity – II. Analysis. J. Mech. Phys. Solids 48, 99–128.
Morris Jr., J.W., Jin, M., Minor, A.M., 2007. In situ studies of the transmission of strain across grain boundaries. Mater. Sci. Eng. A 462, 412–417.
Kochmann, D.M., Le, K.C., 2008. Dislocation pile-ups in bicrystals within continuum dislocation theory. Int. J. Plast. 24, 2125–2147.
Krishnan, J., Steigmann, D.J., 2014. A polyconvex formulation of isotropic elastoplasticity theory. IMA J. Appl. Math. 79, 722–738.
Kröner, E., et al., 1981. Continuum theory of defects. In: Balian, R., et al. (Eds.), Les Houches, Session XXXV, 1980 –Physique des Défauts. North-Holland Publishing Company, pp. 215–315.
Legros, M., Gianola, D.S., Hemker, K.J., 2008. In situ TEM observations of fast grain-boundary motion in stressed nanocrystalline aluminum films. Acta Mater. 56, 3380–3393.
Mazzoni-Leduc, L., Pardoen, T., Massart, T.J., 2008. Strain gradient plasticity analysis of transformation induced plasticity in multiphase steels. Int. J. Solids Struct. 45, 5397–5418.
Noll, W., 1967. Materially uniform simple bodies with inhomogeneities. Arch. Ration. Mech. Anal. 27, 1–32.
Nye, J.F., 1953. Some geometrical relations in dislocated crystals. Acta Metall. 1, 153–162.
Pardoen, T., Massart, T.J., 2012. Interface controlled plastic flow modelled by strain gradient plasticity theory. C.R. Mec. 340, 247–260.
Polizzotto, C., 2009. Interfacial energy effects within the framework of strain gradient plasticity. Int. J. Solids Struct. 46, 1685–1694.
Puri, S., Das, A., Acharya, A., 2011. Mechanical response of multicrystalline thin films in mesoscale field dislocation mechanics. J. Mech. Phys. Solids 59, 2400–2417.
Rupert, T.J., Gianola, D.S., Gan, Y., Hemker, K.J., 2009. Experimental observations of stress-driven grain boundary migration. Science 326, 1686–1690.
Shu, J.Y., Fleck, N.A., 1999. Strain gradient crystal plasticity: size dependent deformation of bicrystals. J. Mech. Phys. Solids 47, 186–213.
Sutton, A.P., Balluffi, R.W., 2003. Interfaces in Crystalline Materials. Clarendon Press, Oxford.
Voyiadjis, G.Z., Faghihi, D., Zhang, Y., 2014. A theory for grain boundaries with strain-gradient plasticity. Int. J. Solids Struct. 51, 1872–1889.
Winning, M., Gottstein, G., Shvindlerman, L.S., 2001. Stress induced grain boundary motion. Acta Mater. 49, 211–219.
Wulfinghoff, S., Bayerschen, E., Böhlke, T., 2013. A gradient plasticity grain boundary yield theory. Int. J. Plast. 51, 33–46.
Wulfinghoff, S., Forest, S., Böhlke, T., 2015. Strain gradient plasticity modeling of the cyclic behavior of laminate microstructures. J. Mech. Phys. Solids 79, 1–20.
Zhang, X., Aifantis, K.E., 2015. Examining the evolution of the internal length as a function of plastic strain. Mater. Sci. Eng., A 631, 27–32.
Zhang, X., Aifantis, K.E., Ngan, A.H.W., 2014a. Interpreting the stress-strain response of Al micropillars through gradient plasticity. Mater. Sci. Eng. A 591, 38–45.
Zhang, X., Aifantis, K.E., Senger, J., Weygand, D., Zaiser, M., 2014b. Internal length scale and grain boundary yield strength in gradient models of polycrystal plasticity: how do they relate to the dislocation microstructure? J. Mater. Res. 29, 2116–2128.

Please cite this article as: A. Basak, A. Gupta, Influence of a mobile incoherent interface on the strain-gradient plasticity of a thin slab, International Journal of Solids and Structures (2016), http://dx.doi.org/10.1016/j.ijsolstr.2016.12.004